理學博士學位論文

Structural Insights into the Interaction between AAA^{+} ATPase p97/VCP and its Substrate Processing Factor, OTU1

2014年 8月

서울大學校 大學院
化學部 生化學專攻
김 수 진

Structural Insights into the Interaction between AAA$^+$ ATPase p97/VCP and its Substrate Processing Factor, OTU1

指導敎授 徐 世 源

이 論文을 理學博士學位 論文으로 提出함.

2014年 6月

서울 大學校 大學院

化學部 生化學專攻

김 수 진

김수진의 理學博士學位 論文을 認准함.

2014年 6月

委 員 長 박승범 印

副委員長 서세원 印

委 員 박충모 印

委 員 김은경 印

委 員 양진국 印

Structural Insights into the Interaction between AAA$^+$ ATPase p97/VCP and its Substrate Processing Factor, OTU1

Thesis by

Su Jin Kim

Professor: Se Won Suh

A Thesis Submitted to the Graduate Faculty of Seoul National University in Partial Fullfillment of the Requirement for the Degree of Doctor of Philosophy

2014

Abstract

The multifunctional AAA^+-ATPase p97/valosin-containing protein (VCP) facilitates essential cellular quality control processes upstream of the proteasome, including endoplasmic reticulum-associated degradation (ERAD). In particular, VCP extracts ubiquitinated protein from macromolecular complexes by utilizing ATP-driven conformational changes in ERAD. Various human diseases from neurodegenerative diseases to cancer are caused by malfunction of components in ERAD. Recently, ERAD-specific deubiquitinating enzymes have been reported to be physically associated with VCP, although the exact mechanism is not yet clear. Among these enzymes is ovarian tumor domain-contain-ing protein 1 (OTU1). OTU1 interacts with VCP via the ubiquitin regulatory X-like (UBXL) domain and deubiquitinates substrates via an ovarian tumor (OTU) domain. However the exact mechanism has not been well understood. Here, the crystal structure of the UBXL domain of OTU1 ($UBXL_{OTU1}$) complexed to the N-terminal domain of VCP (N_{VCP}) is reported at 1.8 Å-resolution. $UBXL_{OTU1}$ adopts a ubiquitin-like fold and binds at the interface of two subdomains of N_{VCP} using the ^{39}GYPP^{42} loop of $UBXL_{OTU1}$ with the two prolines in cis- and trans-configurations, respectively. A mutagenesis study shows that this loop is not only critical for the interaction with VCP but also for its role in the ERAD pathway. Negative staining EM shows that one molecule of OTU1 binds to one VCP hexamer, and isothermal titration calorimetry suggests that the two proteins bind with a K_D of 0.71 μm. Analytical size exclusion chromatography and isothermal titration calorimetry demonstrates that OTU1 can bind VCP in both the presence and absence of a heterodimer formed by ubiquitin fusion degradation protein 1 and nuclear localization protein 4. Taken together, the structure reveals that UBXL is another cofactor of VCP having its own

specific characteristics. In addition, the interaction between VCP and OTU1 is specific and critical in ERAD.

Key words: ER-associated degradation/ VCP/ OTU1/ Protein-protein interaction/ Crystal structure/ Electron microscopy/ Isothermal titration calorimetry/ Site directed mutagenesis

Table of Contents

List of Tables

List of Figures

Abbreviations

AAA	ATPases associated with various cellular activities
ALS	amyotrophic lateral sclerosis
ATP	adenosine triphosphate
BS1	Binding Site 1
CAD	chromatin-associated protein degradation
CDC48	cell division protein 48
CFTR	cystic fibrosis transmembrane conductance regulator
DPBS	Dulbecco's phosphate-buffered saline
DUB(s)	deubiquitinating enzyme(s)
EM	Electron microscopy
ERAD	endoplasmic reticulum-associated degradation
GST	glutathione S transferase
IBMPFD	incusion body myopathy with Paget disease of bone and frontotemporal dementia
IPTG	isopropyl β-D-thiogalactopyranoside
ITC	Isothermal titration calorimetry
MR	molecular replacement
NPL4	nuclear localization protein 4
OTU	ovarian tumor
OTU1	OTU domain containing protein 1
PMSF	phenylmethylsulfonyl fluoride
PUB	PNGase/UBA or UBX

PUL	human PLAP and homologous UFD3/DOA1 in *Saccharomyces cerevisiae* and LUB1 in *Schizosaccharomyces pombe*
RAD	ribosome-associated degradation
RMSD	root-mean-square deviation
RPN-I	ribophorin I
SMD	Solvation Model based on Density
TCEP	Tris(2-carboxyrthyl) phosphine hydrochloride
TCR_{α}	T-cell receptor alpha
UBA	ubiquitin-associated
UBD	ubiquitin D
UBL	ubiquitin-like
UBX	ubiquitin regulatory X
UBXL	UBX-like
UBX proteins	UBX domain-containing proteins
UFD1	ubiquitin fusion degradation protein 1
VBM	VCP-binding motif
VCIP135	VCP complex-interacting protein of 135 kDa
VCP	valosin-containing protein
VIM	VCP-interacting motif
VIMP	VCP interacting membrane protein
WT	wild type
ZnF	zinc finger

1. Introduction

The molecular chaperone valosin-containing protein (VCP) - also known as p97 and cell division cycle 48 (CDC48) - is an essential and highly abundant type II AAA (ATPase associated with a variety of activities) ATPase, comprising approximately 1% of the cytosol. It is composed of an N-terminal domain, two ATPase domains (D1 and D2), and an unstructured C-terminal tail. It forms a homohexameric ring structure with D1 and D2 stacked in a head to tail manner, and the N-terminal domains are enclosed by the D1 ring (Zhang et al., 2000; DeLaBarre and Brunger, 2003) (Figure 1). It is conserved from archaea to mammals and participates in a variety of cellular processes involving protein ubiquitylation, including protein quality control, cell cycle progression, autophagy, homotypic membrane fusion, transcriptional activation, DNA damage repair, apoptosis, endosomal sorting, and regulation of protein degradation at the outer mitochondrial membrane (Woodman, 2003; Wang et al., 2004; Meyer et al., 2012, and reference therein). Within these processes, VCP acts as a molecular segregase that utilizes ATP-powered conformational changes in the assembly and disassembly of macromolecular machineries (Halawani and Latterich, 2006; Jentsch and Rumpf, 2007). ATP hydrolysis in the D2 ring of VCP is major ATPase activity, while the D1 ring is involved in the regulation of VCP hexamerization (Song et al., 2003). It is not surprising that defects in VCP contribute to various neurodegenerative diseases such as Alzheimer's (Halawani et al., 2010), Parkinson disease, and cancer (Chapman et al., 2011). Recently, it has been reported that mutations in VCP can cause incusion body myopathy with Paget disease of bone and frontotemporal dementia (IBMPFD) as well as familial amyotrophic lateral sclerosis (ALS) (Yamanaka et al., 2012; Erzurumlu et al., 2013).

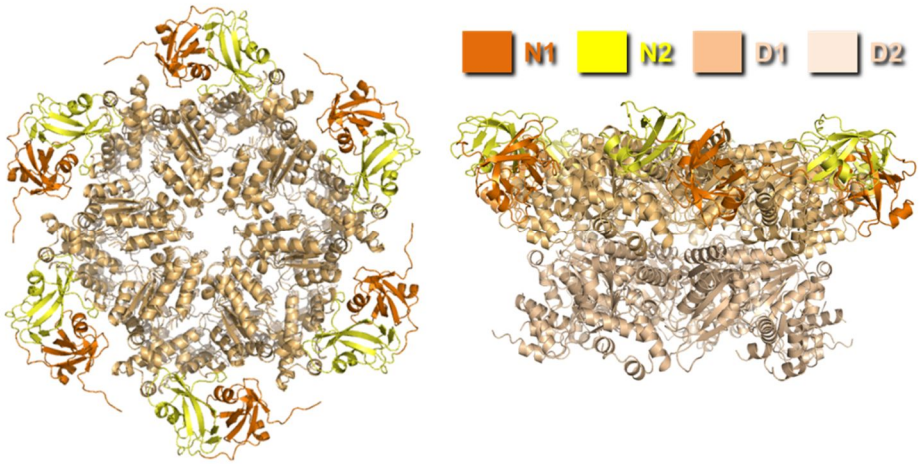

Figure 1. Structure of VCP (PDB code: 1R7R)

The hexamer is viewed from left (top) and right (side). Different colors represent the main domains (N, D1, and D2). The image was generated using PyMOL (DeLano, 2002).

The diverse biological functions of VCP are controlled by many binding partners that recruit specific ubiquitinated substrates to VCP by altering their ubiquitination state (Rumpf and Jentsch, 2006; Schuberth and Buchberger, 2008) (Figure 2). Most binding partners interact with VCP through a limited set of binding modules. An ubiquitin regulatory X (UBX) domain is the most studied binding domain, which binds to the N-terminal domain of VCP (Schuberth and Buchberger, 2008). Binding partners containing PUB (PNGase/UBA or UBX) or PUL (human PLAP and homologous UFD3/DOA1 in *Saccharomyces cerevisiae* and LUB1 in *Schizosaccharomyces pombe*) domains bind to the C-terminal tail of VCP (Yeung et al., 2008; Buchberger, 2010). In addition to these domains, several short, linear binding motifs of binding partners mediating binding to the N-terminal domain of VCP have been identified, including Binding Site 1 (BS1; also known as SHP box) in UFD1 and p47 (Bruderer et al., 2004; Hitt et al., 2004; Sato and Hampton, 2006), the VCP-binding motif (VBM) in E4B/UFD2, HRD1, and Ataxin-3 (Boeddrich et al., 2006), and the VCP-interacting motif (VIM) in SVIP and GP78 (Ballar et al., 2006). They can be classified as substrate recruiting and substrate processing factors according to their roles (Jentsch and Rumpf, 2007). Substrate recruiting factors harbor ubiquitin association domains and do not possess enzyme activities. Substrate processing factors possess enzymatic activity (and in many cases, ubiquitin binding domains as well) and can modify substrates by ubiquitination (*e.g.* E4B/UFD2 and perhaps RING finger 31), deubiquitination- *e.g.* YOD1, VCP complex-interacting protein 135 kDa (VCIP135), and Ataxin-3- and in the case of PNGase, deglycosylation.

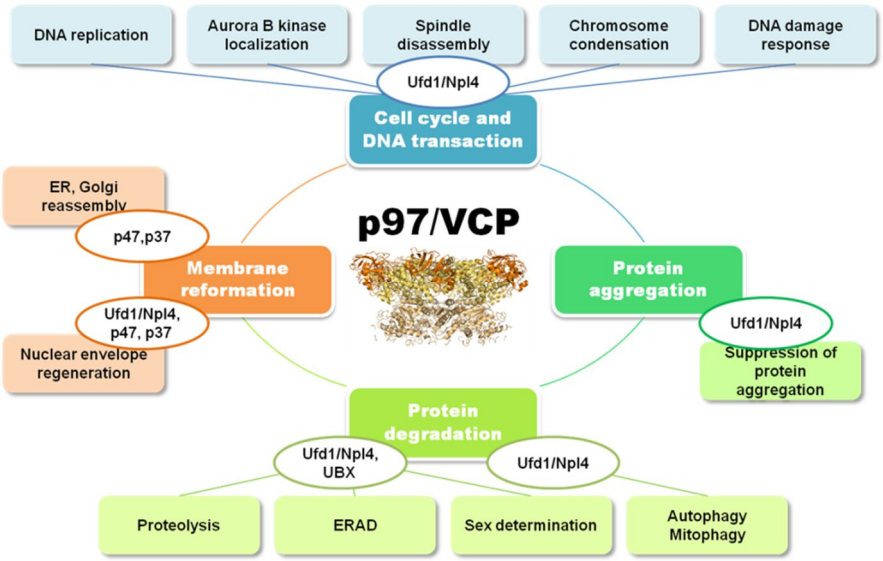

Figure 2. Multiple functions of VCP

UBX is the most prominent VCP interacting domain and has a similar fold to ubiquitin, but they lack sequence homology. There are at least 13 different UBX domain-containing proteins (UBX proteins) in mammalian cells, and their functions are largely uncharacterized. All UBX proteins were recently shown to interact with VCP as major regulators of VCP function (Alexandru et al., 2008; Schuberth and Buchberger 2008). It is not known how many different complexes of VCP and binding partners exist in the cell, but current understanding of VCP and its binding partners suggests the existence of the following three primary mutually exclusive complexes of VCP and binding partner: VCP-UFD1/NPL4, VCP-p47, and VCP-UBXD1 (Meyer et al., 2012). Each of the complexes is dedicated to a specific ubiquitin-dependent cellular process. According to the previous reports, the VCP-UFD1/NPL4 complex is involved in regulating mostly Lys48-polyubiquitinated substrates and proteasomal degradation in diverse cellular processes, such as the endoplasmic reticulum-associated degradation (ERAD), chromatin-associated protein degradation (CAD), or ribosome-associated degradation (RAD). In contrast, VCP-p47 and VCP-UBXD1 complexes are involved in ubiquitin-dependent proteasome-independent membrane fusion and vesicular trafficking processes (Hänzelmann et al., 2011).

Considerable progress has been made in characterizing the functional contribution of VCP in ERAD and has been reviewed previously (Hirsch et al., 2007; Raasi and Wolf, 2007). Briefly, the ER is the first compartment in the secretory pathway. Protein destined for the secretory pathway are translocated into the lumen or inserted into the membrane of the ER where they are properly folded and modified before being delivered to their functional destination (Federovitch et al., 2005; Levine and Rabouille, 2005). However, protein folding in the secretory pathway is an imperfect process that generates products (Hampton, 2002; Meusser et al., 2005). Terminally misfolded or unassembled proteins that are unable to acquire their native structure must be degraded to prevent fruitless folding attempts and the accumulation of misfolded polypeptides

in the ER. This degradation process is ERAD as a quality control mechanism (DeLaBarre and Brunger, 2003; de Vrij et al., 2004; Bagola et al., 2011; Wolf and Stolz, 2012). ERAD belongs to the ubiquitin-proteasome pathway requiring two catalyzing processes, ubiquitination which requires three enzymes, an E1 ubiquitin activating, an E2 ubiquitin conjugating enzyme, and an E3 ubiquitin ligase and deubiquitination is carried out by the deubiquitinating enzymes (DUBs) (de Vrij et al., 2004). It has been shown that Lys48- and Lys11-linked ubiquitin chains can serve as proteasomal degradation signals for a subset of substrates in ERAD (Xu et al., 2009). This pathway occurs in three steps: (1) recognition and targeting (substrate recognition within the ER and targeting to the retrotranslocon), (2) retrotranslocation (substrate delivery from the ER to the cytosol), and (3) degradation by the proteasome (Hegde and Ploegh 2010). Proteins that are subjected to ERAD can be classified with respect to the location of their misfolded domain(s) relative to the ER membrane. Interestingly, in yeast and mammalian cells, there is a clear correlation between the location of the misfolded domain and theERAD complex for degradation. Membrane proteins with misfolded cytosolic domains are degraded via the DOA10-complex, the pathway was termed ERAD-C (C for cytosolic) (Vashist and Ng, 2004). Conversely, membrane proteins with misfolded luminal domains are degraded via the HRD1-complex, this pathway was named ERAD-L pathway (L for luminal) (Vashist and Ng, 2004). Finally, proteins with misfolded transmembrane regions are degraded via the HRD1-complex with fewer components, this pathway was termed ERAD-M (M for membrane) (Carvalho et al., 2006; Hom et al., 2009; Sato et al., 2009). Soluble misfolded luminal proteins are degraded via the ERAD-L pathway.

In ERAD, VCP functions at the cytosolic phase of the retrotranslocation channel and couples substrate retrotranslocation to its ubiquitination and subsequent degradation by the proteasome (Ye et al., 2001; Jarosch et al., 2002). The role of VCP in ERAD is mediated by several binding partners (Figure 3). VCP is tethered to the ER membrane via binding to HRD1

and, independently, via binding to its binding partner and integral membrane protein UBX2, which is part of both the HRD1 and DOA10-complexes. VCP engages ubiquitinated proteins via a heterodimeric complex comprised of nuclear localization protein 4 (NPL4) and ubiquitin fusion degradation protein 1 (UFD1). These proteins support binding to ubiquitin through specific domains, although they are not completely conserved. NPL4 possesses a zinc finger motif whereas UFD1 has a conserved UT3 motif. Membrane-anchored auxiliaries such as Derlin-1 (DER1), a candidate ER-retrotranslocation channel analogous to SEC61 (Lilley and Ploegh, 2004; Ye et al., 2004), VCP interacting membrane protein (VIMP), a transmembrane protein with a lengthy cytosolic C-terminal domain (Ye et al., 2004), UBXD2 (Rape et al., 2001; Park et al., 2005), and UBXD8 (Ye et al., 2003) may recruit VCP to the ER membrane. PNGase (PNG1) is deglycosylates misfolded glycoproteins (Kim et al., 2006) and E4B/UFD2 is responsible for further substrate polyubiquitination and enhanced proteasome delivery (Nakatsukasa et al., 2008). DUBs such as Ataxin-3, USP19, and YOD1 are required for ERAD (Wang et al., 2006; Zhong and Pittman, 2006; Hassink et al., 2009; Ernst et al., 2009). Ubiquitinated substrates are transferred to the proteasome by shuttle proteins, known as HR23A/B or Ubiquilin-1 (RAD23 and DSK2 in yeast), which contain ubiquitin-associated (UBA) and ubiquitin-like (UBL) domains that bind to polyubiquitin chains and the proteasome subunits (RPN10/13, RPT5), respectively (Finley, 2009; Lim et al. 2009). Although there is now good information pertaining to the number, types, and activities of proteins involved in ERAD, there are still many unresolved issues.

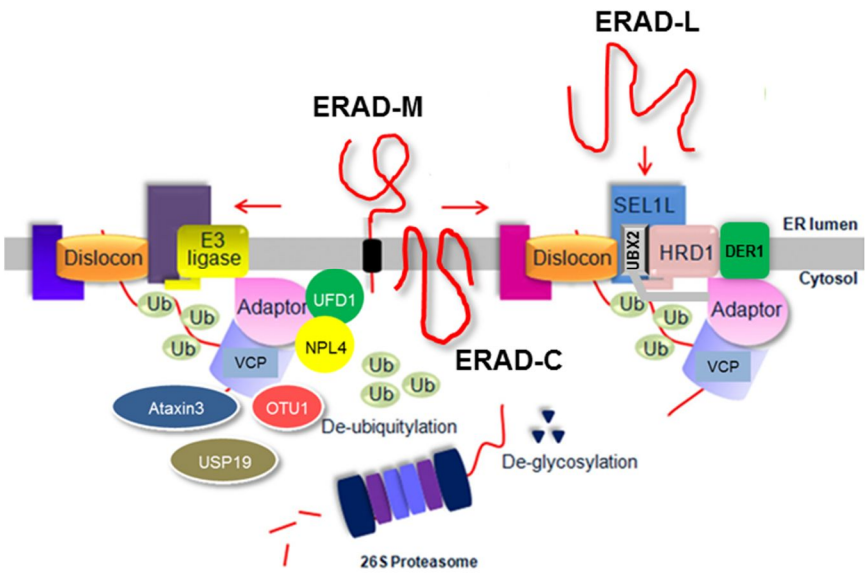

Figure 3. ERAD pathway

Substrate-specific ERAD pathways (Merulla et al., 2013)

Above all, ERAD is required polyubiquitin chains with optimal length and linkage for proteasomal targeting, adding weight to the importance of substrate processing factors of VCP. It has been put considerable emphasis on the roles of DUBs at are taken into account regulation of substrate stability by editing ubiquitin chains on substrates in ERAD pathway recently. As mentioned above, there are three ERAD-associated DUBs, Ataxin-3, USP19, and YOD1. More direct support for a role of DUBs in ERAD comes from studies in the mammalian system. For instance, Ataxin-3, which is involved in the neurodegenerative disease spinocerebellar ataxia, is needed for transfer of substrates from VCP to the proteasome (Wang et al., 2006; Zhong and Pittman, 2006). Another example is the ER membrane anchored USP19, which results in the blockage of ERAD of unassembled T-cell receptor alpha (TCR_{α}) and cystic fibrosis transmembrane conductance regulator (CFTR)ΔF508 upon overexpression, a condition that also leads to ER stress (Hassink et al., 2009). Finally, YOD1, a member of the mammalian otubain family of DUB and is involved in retrotranslocation and degradation of misfolded ER luminal and membrane proteins (Ernst et al., 2009). YOD1, a human homologue of the ovarian tumor domain-containing protein 1 (OTU1) from *S. cerevisiae*, contains three domains: an N-terminal ubiquitin regulatory X-like (UBXL) domain, the OTU domain, and a C-terminal zinc finger (ZnF) domain of unknown function. The OTU domain of which plays a role as a substrate processing factor of VCP by executing the removal of ubiquitin chains that belongs to the OTU domain proteases such as papain-like cysteine DUBs, which have been found in eukaryotes, bacteria, and viruses (Makarova et al., 2000). It directly binds to VCP via the UBXL domain and leads dislocation of substrate by interacting with dislocation machinery components such as Derlin-1 and UBXD8. It has been also reported that the abrogation of deubiquitinating activity resulted in impairment of the degradation of misfolded RI332 as an ERAD substrate, contributing to positive regulation in ERAD pathway (Ernst et al., 2009). Interference with dislocation/VCP-associated deubiquitinaing activity causes accumulation of

misfolded proteins at a step before membrane extraction. However, it remains unclear what the precise mode of action.

The UBXL domain of OTU1 ($UBXL_{OTU1}$) consists of about 80 residues similar to the UBX but has low sequence identity of less than 15% or so to UBX. The UBX is the representative binding module of VCP, *i.e.* it interacts with N_{VCP} via conserved residues which are arginine from strand β1 and the three residues (Phe-Pro-Arg) in a four-residues-long loop formd between strands β3 and β4 often referred to as the S3/S4 loop (Schuberth and Buchberger, 2008; Kloppsteck et al., 2012). These conserved residues are called the signature motif (R…FPR) of UBX. However OTU1 does not have the signature motif of UBX-thereby it is expected to bindto VCP differently from UBX. So far, the structure of the OTU domain from yeast complexed with ubiquitin has been produced (Messick et al., 2008; PDB code: 3BY4), and recently it has been published that human OTU1 has high specificity for Lys11-linked ubiquitin chains in a report that shows the complex structure of OTU1 with Lys11-linked diubiquitin (Mevissen et al., 2013; PDB code: 4BOQ, and 4BOZ). To understand how OTU1 interacts with VCP on a molecular level and to gain insight into how this interaction regulates ERAD, a structural study on N_{VCP} complexed with $UBXL_{OTU1}$ was carried out, and negative staining electron microscopy (EM) and biochemical studies of the full-length proteins were also performed.

2. Materials and Methods

2.1. Cloning, Mutagenesis, and Protein Preparation

All human VCP and yeast OTU1 proteins were cloned into the expression vector pET28a (Novagen) that appends an N-terminal histidine tag and thrombin site to the target protein under T7 promoter control. All proteins used in this study are shown in Figure 4. Substitution of Gly-Tyr-Pro-Pro to Thr-Phe-Pro-Arg at positions 39–42 of the full-length OTU1 (residues 1–301) was introduced by a PCR method in clone OTU1 ^{39}TFPR^{42}. For expression in mammalian cells, the constructs encoding pCS2-HA-OTU1 WT and pCS2-HA-OTU1 ^{39}TFPR^{42} were prepared. A ribophorin I mutant (RPN-I^{N299T}) with the asparagine at position 299 replaced by threonine was cloned into the pEGFP-C1 vector (Clontech). For analytical size exclusion chromatography, the full-length UFD1 (residues 1–307) and NPL4 (residues 1–608) were cloned into the pET28a and pET22b vectors (Novagen), respectively, which are named pET28a-UFD1 and pET22b-NPL4. The glutathione S-transferase (GST) protein was fused to the N terminus of the full-length OTU1, and pGST-OTU1 was derived from pGEX-4T-1 (GE Healthcare). All proteins were expressed in *Escherichia coli* Rosetta (DE3). Cells were grown in LB medium at 37 °C, and protein expression was induced by 0.5 mM isopropyl β-$_D$-1-thiogalactopyranoside at 18 °C overnight. Harvested cells were lysed in buffer A (20 mM Tris hydrochloride, pH 8.0, 100 mM sodium chloride, 0.5 mM tris (2-carboxyethyl) phosphine with 1 mM PMSF) and purified using nickel-nitrilotriacetic acid (Ni-NTA) affinity chromatography (GE Healthcare). Afterward, the histidine tag was proteolytically cleaved by addition of thrombin (Enzyme Research Laboratories), and protein was further purified using size exclusion chromatography on a HiLoad Superdex 75 or 200 26/60 column (GE Healthcare) in buffer A or buffer B (20 mM HEPES, pH 7.5, 150 mM sodium chloride). 2 mM ATP and 5 mM magnesium chloride were

added to the full-length VCP (residues 1–806). A UFD1/NPL4 heterodimeric complex was formed by mixing pET28a-UFD1 and pET22b-NPL4. For the formation of complexes using the full-length proteins, VCP and either OTU1 (VCP/OTU1) or UFD1/NPL4 (VCP·UFD1/NPL4) were incubated at a molar ratio of 1:3 for 1 h at 4 °C, and then VCP/OTU1 and VCP·UFD1/NPL4 complexes were analyzed by size exclusion chromatography.

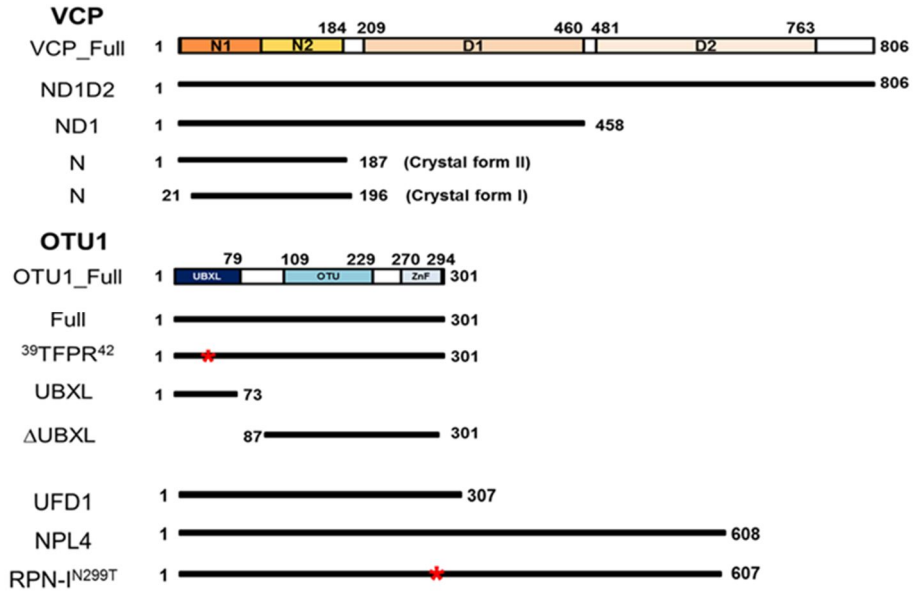

Figure 4. Schematic representation of proteins used in this study

The mutation site is indicated by asterisks.

2.2. Limited Proteolysis of the Complex of N_{VCP} and $UBXL_{OTU1}$

Purified complexes of N_{VCP} and the $UBXL_{OTU1}$ were digested with chymotrypsin and trypsin (Sigma) at a protein-to-protease ratio of 1,000:1 in buffer A for 15 and 5 min, respectively, at 37 ℃. The reactions were stopped by addition of 0.1 mM PMSF. Reaction products were resolved by 15% SDS-PAGE and visualized by subsequent Coomassie Brilliant Blue staining. The proteins were used at a concentration of 20 mg/ml for crystallization.

2.3. Crystallization of the VCP and OTU1 Complex

Crystals of crystal form I were obtained from a reservoir solution containing 14% PEG 4000, 100 mM sodium acetate, pH 5.0, and those of crystal form II were obtained from 20% PEG 2000, 10% tacsimate, pH 5.0 using the hanging drop vapor diffusion method by mixing with an equal volume of the protein solution (Figure 5). Crystals in a soaking solution containing 25% ethylene glycol as a cryoprotectant were flash cooled in liquid nitrogen.

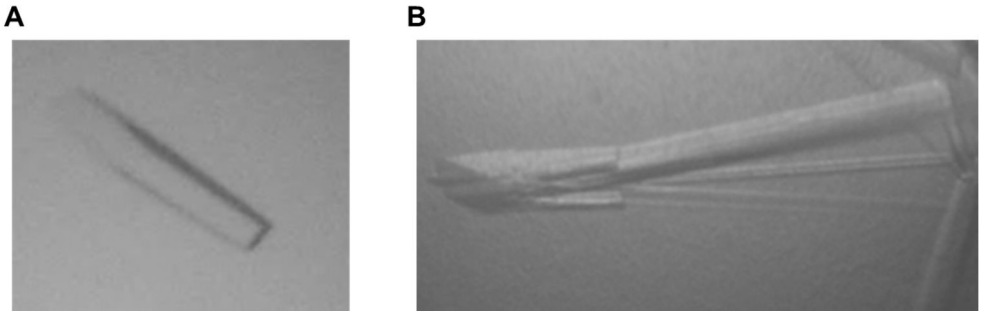

Figure 5. Crystals of VCP and OTU1 complex

(A) A crystal from crystal form I with approximate dimensions of 0.3 mm x 0.05 mm x 0.05 mm. (B) A crystal from crystal form II with approximate dimensions of 0.5 mm x 0.1 mm x 0.05 mm.

2.4. Data Collection and Structure Determination

Diffraction data of two crystal forms were collected at 100 K on the beamline 5C of Pohang Light Source, Korea. The data were processed and scaled using the program suit HKL2000 (Otwinowski and Minor, 1997). Crystal form I in the asymmetric unit was located by Molecular Replacement using the program PHASER (McCoy et al., 2007), with the free VCP structure (Zhang et al., 2000, PDB code: 1E32) as a search model. The structure of crystal form II was subsequently determined using the refined structure of crystal form I as an input model. The initial model was subjected to iterative cycles of model building by placing manually into the unoccupied densities with COOT (Emsley and Cowtan, 2004), and refinement was carried out by CNS (Brunger et al., 1998), PHENIX (Zwart et al., 2008), and REFMAC5 (Murshudov et al., 1997). Water molecules were added with COOT, and structures of two crystal forms were validated using PROCHECK (Laskowski et al., 1993). All figures were generated with PyMOL (DeLano, 2002). The data collection and processing statistics for two structures are summarized in Table 1.

Table 1. Data collection and refinement statistics: VCP-OTU1 complex

	Crystal form I	Crystal form II
Data sets		
Beam line	PAL 5C (SB II)	
X-ray wavelength (Å)	0.97951	0.97951
Resolution range (Å)	50.00-1.81(1.87-1.81) [a]	50.00-1.86(1.93-1.86) [a]
Space group	$P2_12_12_1$	$P2_12_12_1$
Unit cell parameters (Å)	a=43.604, b=60.803, c=111.915, α=90.000, β=90.000, γ=90.000	a=42.819, b=88.609, c=143.535, α=90.000, β=90.000, γ=90.000
Z	1	2
Total/unique reflections (N)	684606/27896	1413706/46883
Completeness (%)	99.3(99.6) [a]	96.5(88.9) [a]
Mean I/σ (%)	23.8(8.9) [a]	25.0(2.6) [a]
R_{merge} [a] (%)	9.1(25.2) [a]	8.9(38.5) [a]
Refinement statistics		
No. of atoms	2206	3872
No. of water molecules	272	198
Resolution range (Å)	33.78-1.81	42.34-1.86
R/R_{free} [b] (%)	18.24/21.34	21.37/25.68
R.m.s. deviations bond length (Å)/angle(degrees)	0.026/2.145	0.023/1.926
Average B-factor (Å^2)	18.98	30.61
Ramachandran Plot		
Favored region (%)	98.7	96.7
Allowed region (%)	1.3	3.3
Disallowed region (%)	0	0

[a] Values in parentheses refer to the highest resolution shell.

[b] $R_{merge} = \sum_h\sum_i|I(h,i)| <I(h)>|/\sum_h\sum_i I(h,i)$, where I(h,i) is the intensity of the ith measurement of reflection h, and $<I(h)>$ is the mean value of $I(h,i)$ for all i measurements.

[c] R_{free} was calculated from the randomly selected 10% set of reflections not included in the calculation of the R value.

2.5. Computational Methods

A model peptide Ac-Arg-Phe-Gly-Tyr-Pro-Pro-Gln-Arg-NHMe which corresponds to the S3/S4 loop of OTU1 was built using an X-ray structure of crystal form I. The structure was optimized at the M06-2X/6-31G(d) level of theory in water and its solvation free energy was calculated using the Solvation Model based on Density (SMD) method (Marenich et al., 2009). All quantum mechanical calculations were carried out using the Gaussian 09 package (Frisch et al., 2009).

2.6. Chemical Cross-linking

VCP·UFD1/NPL4 complex was purified and concentrated to 0.05 mg/ml in buffer B. To improve its stability, the complex was chemically cross-linked with a final concentration of 0.1% EM grade glutaraldehyde (Sigma) for 10 min at 25 ℃. The reaction was stopped by adding Tris, pH 8.0 to a final concentration of 25 mM.

2.7. Isothermal Titration Calorimetry (ITC) Measurements

ITC experiments were performed on an iTC200 calorimeter (GE Healthcare) at 25 ℃. For the interaction between the full-length VCP and OTU1, OTU1 wild type (WT) or the mutant (^{39}TFPR^{42}) was placed in the syringe at 300 or 500 μM, respectively, and injected into the sample cell containing the full-length VCP ($Full_{VCP}$) at a concentration of 13 μM. Titrations of each $\Delta UBXL_{OTU1}$ (500 μM) into $Full_{VCP}$ (50 μM) and $UBXL_{OTU1}$ (1000 μM) into N_{VCP} (80 μM) were also performed. The concentration of VCP/OTU1 and VCP·UFD1/NPL4 complexes was 0.01 μM in the sample cell, and UFD1/NPL4 and OTU1 were titrated to a concentration of 20 μM. The buffer B always matched between the syringe and the sample cell. The data were analyzed with the software Origin 7.0 using a one-site model.

2.8. In vitro Assays of Substrate Degradation

HEK293T cells were seeded onto 12-well poly-L-lysine-coated plates at a density of 2.5 × 10^5 cells/well, and then transfection with expression plasmids was performed for 2 days using Effectene reagent (Qiagen). The total amount of DNA used in each well for transfection was 600 ng. Cells were treated with 10 μM MG132 for 2 h to prevent protein degradation and washed twice with complete medium. After addition of cycloheximide at a final concentration of 100 μg/ml, cells were harvested with cold Dulbecco's phosphate-buffered saline (PBS) and lysed, and cell extracts were analyzed by Western blotting with antibodies against pCS2-HA, pCS2-HA-OTU1 WT, pCS2-HA-OTU1 ^{39}TFPR^{42}, and pEGFP-C1-RPN-I^{N299T}.

2.9. Ni-NTA Nanogold Labeling of VCP and OTU1 Complex

The complex was prepared by co-purifying the full-length untagged VCP and OTU1 tagged with a hexahistidine tag at the C terminus. Freshly purified protein complex and 5-nm-diameter Ni-NTA Nanogold (Nanoprobes Inc.) were incubated together at a molar ratio of 1:10 for 10 min at 4 °C. The mixture was purified with a further chromatographic step using a Superdex 200 10/300 GL column (GE Healthcare) in buffer A. Excess Ni-NTA Nanogold was removed by centrifugation at 3,000 × *g* for 15 min using a 10-kDa-cutoff filter (Satorius).

3.0. Electron Microscopy (EM)

The complex of full-length VCP and OTU1 (VCP/OTU1) labeled with gold was diluted to 20 μg/ml in buffer A. The samples were loaded onto a glow-discharged copper grid coated with a carbon film and stained with 2% uranyl acetate solution. Images were recorded on the film using a Tecnai F20 microscope operated at 200 kV equipped with a 2,048 × 2,048-pixel Gatan charge-coupled device camera. The gold-labeled proteins were selected from individual digital micrographs using a semiautomatic selection procedure, and the stoichiometry of OTU1

incorporation into VCP was determined by counting the number of gold particles. For unlabeled VCP/OTU1 complex, VCP/OTU1 complex was formed by incubating purified VCP with a 10-fold molar excess of OTU1 for 15 min at 4 ℃. The complex was then further purified using size exclusion chromatography (GE Healthcare) in buffer containing 20 mM Tris hydrochloride, pH 8.0, 200 mM sodium chloride. 3 μl of VCP/OTU1 complex fraction at 0.1 μM was applied to a glow-discharged carbon-coated copper grid, and negatively stained with 2% methylamine vanadate, pH 8.0 (Nanoprobes Inc.). The specimen was examined under a Tecnai T120 microscope at 120 kV using a nominal magnification of 67,000× (1.64 Å/pixel, FEI Eindhoven, The Netherlands). Images were recorded with an FEI Eagle 4.000 × 4,000-pixel charge-coupled device camera using a defocus of 1.2 μm and an electron dose of about 30 e^-/A^2.

3.1. EM Image Processing

Because VCP has a preferred orientation on the EM grid, we could only obtain the hexagonal view of VCP or VCP/OTU1 complex. Hexagonal particles were automatically selected with EMAN2 boxer, and bad particles were manually excluded (Tang et al., 2007). A total of 2,839 particles were selected from 50 micrographs. Subsequent processing was performed using IMAGIC (van Heel et al., 1996). To separate VCP/OTU1 complex from the heterogeneous data set containing either VCP or VCP/OTU1 complex, comparative projection matching with two reference sets was executed. One reference set was the forward projection of the crystal structure of VCP hexamer (Huyton et al., 2003; Protein Data Bank code 1R7R), and the other reference set was the forward projection of the model structure of VCP hexamer with one OTU1 molecule (Protein Data Bank codes 4KDI and 4KDL in the present work and 1R7R). These two separate data sets were respectively subjected to 10 rounds of reference-free alignment and multivariate statistical analysis followed by multivariate statistical analysis classification and averaging.

3.2. Analytical Size Exclusion Chromatography

pET28a-VCP, pGST-OTU1, pET28a-UFD1, and pET22b-NPL4 were expressed and purified separately. A heterodimeric complex of UFD1/NPL4 was formed by mixing pET28a-UFD1 and pET22b-NPL4. Analytical size exclusion chromatography was carried out at 4 °C on a Superdex 200 10/300 GL column (GE Healthcare) in buffer A at a flow rate of 0.5 ml/min. Elution fractions were analyzed for complexes by SDS-PAGE and Coomassie Brilliant Blue staining.

3. Results and Discussion

3.1. Overall Structure of N_{VCP} and $UBXL_{OTU1}$ Complex

In order to obtain atomic details on the interaction between VCP and OTU1, a number of complexes of VCP and OTU1 using various fragments containing the full-length were subjected to crystallization trials (see Figure 4). However, only complexes of N_{VCP} and $UBXL_{OTU1}$ yielded diffraction quality crystals in two conditions: one with residues 21-196 and the other with residues 1-187 of N_{VCP}, referred to hereafter as crystal form I and crystal form II, respectively (Figure 4). Both crystal form I and II crystallized in space group $P2_12_12_1$, but with $Z = 1$ and $Z = 2$, respectively, and were refined at 1.81- and 1.86-Å resolution, respectively. First, the molecular replacement (MR) method using various structures such as UBX of Fas-associated factor 1 (FAF1) (Protein Data Bank code 3QX1; denoted as UBX_{FAF1} hereafter) and the NMR structure of $UBXL_{OTU1}$ (Protein Data Bank code 2KZR) failed to give a solution. However, repeating the search using uncomplexed N_{VCP} (residues 21-187) (Zhang et al., 2000, PDB code: 1E32) as a search model gave a solution, and the subsequent $F_o - F_c$ difference electron density map revealed unambiguous density for bound OTU1. The structure of crystal form II was determined by the MR method using the structure of crystal from I. Residues that were not visible in the electron density map were left out in the final model; they include residues 1-20 of N_{VCP} in all three molecules, 121-128 of N_{VCP} in one molecule from crystal form II, 48-52 of $UBXL_{OTU1}$ in crystal form I, and 49-55 in one molecule of $UBXL_{OTU1}$ from crystal form II. The statistics on data collection and the refinements are given in Table 1.The overall structure of the N_{VCP} and $UBXL_{OTU1}$ complex is shown in Figure 6. As seen in the figure, N_{VCP} is composed of two subdomains (N1 and N2) connected by a seven-residues-long linker, and $UBXL_{OTU1}$ binds at the interface between the N1 and N2 domains of VCP. The N1

domain (residues 23-104) consists of a double-Ψ β-barrel, and the N2 domain (residues 112-196) consists of a six-stranded β-clam with two helices on the two ends as described earlier (DeLaBarre and Brunger, 2003). The structure of $UBXL_{OTU1}$ (residues 1-73) reveals a β-grasp fold with a β-β-α-β-β-α-α-β secondary structural organization that resembles ubiquitin and ubiquitin-like proteins as well UBX and the ubiquitin D domain (UBD) (Isaacson et al., 2007; Messick et al., 2008). The structure of N_{VCP} in its apo state and in complex with $UBXL_{OTU1}$ can be superposed with a root-mean-square deviation (RMSD) value of 0.53 Å. There are minor conformational changes of N_{VCP} upon $UBXL_{OTU1}$ binding. Glu34, Pro106, Asp107, Met158 of N_{VCP} show alternate side chain conformations (Figure 7). However all are away from the interaction interface so that they are not involved in the interaction with $UBXL_{OTU1}$.

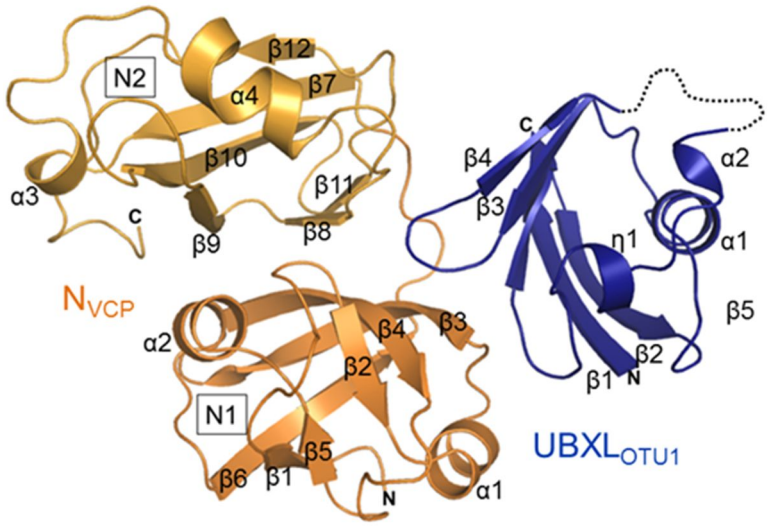

Figure 6. Overall structure of N_{VCP} and $UBXL_{OTU1}$ complex

Ribbon presentation of $UBXL_{OTU1}$ in complexed with N_{VCP} is shown in blue and orange, respectively. Secondary structure elements are labeled as α-helix in α, β-strand in β, and 3_{10}-helix in η. Disordered regions are indicated by dotted lines.

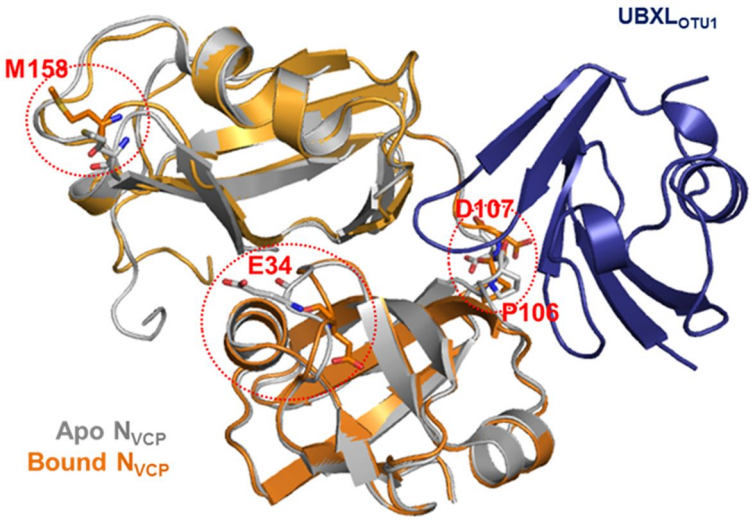

Figure 7. Conformational change on N_{VCP} upon $UBXL_{OTU1}$ binding

Superposition of N_{VCP} in the apo state (gray) and in complex (orange) with $UBXL_{OTU1}$ (blue). The side chains of Glu34, Pro106, Asp107, and Met158 are shown in stick representation.

3.2. Comparison of Three Crystallographically Independent Molecules

The three crystallographically independent molecules, one from crystal form I and two from crystal form II, are almost identical (Figure 8). When the molecule of crystal form I is taken as a reference, the two molecules in crystal form II show RMSD values of 0.63 and 0.64 Å for N_{VCP} and 0.45 and 0.50 Å for $UBXL_{OTU1}$. In the case of N_{VCP}, residues 33-34, 119-129, 155-159, and 182-187 show RMSD values greater than 3 Å (Figure 9A), but they are typically located on the surface away from the binding interface with $UBXL_{OTU1}$. These high RMSD values are due to differences in the crystal packing environment or flexibility of the molecule. They form ten hydrogen bonds and four salt bridges with the N2 domain of neighboring N_{VCP} molecule (Figure 9B). Residues 46–56 are ordered in only one of the three $UBXL_{OTU1}$ molecules because there is a neighboring molecule stabilizing the structure by forming hydrogen bonds (Figure 9B). Conversely, the superposition of $UBXL_{OTU1}$ with the earlier reported NMR structure (Protein Data Bank code 2KZR) gives an RMSD value of 2.18 Å for 73 Cα atoms; this might be the reason for the failure to obtain a solution using the structure as a search model.

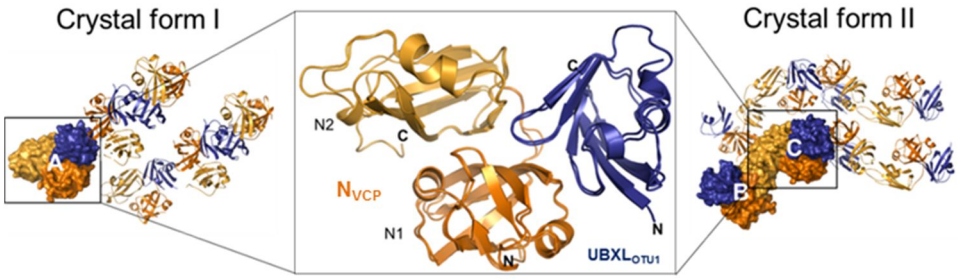

Figure 8. Comparison of Two Crystal Forms

Molecular packing in the crystal forms I (left) and II (right) are shown with VCP and OTU1 in orange and blue, respectively. Superposition of the molecules in two crystal forms is shown in the middle. Molecules in the asymmetric unit are shown in surface while the neighboring molecules are in ribbon representation.

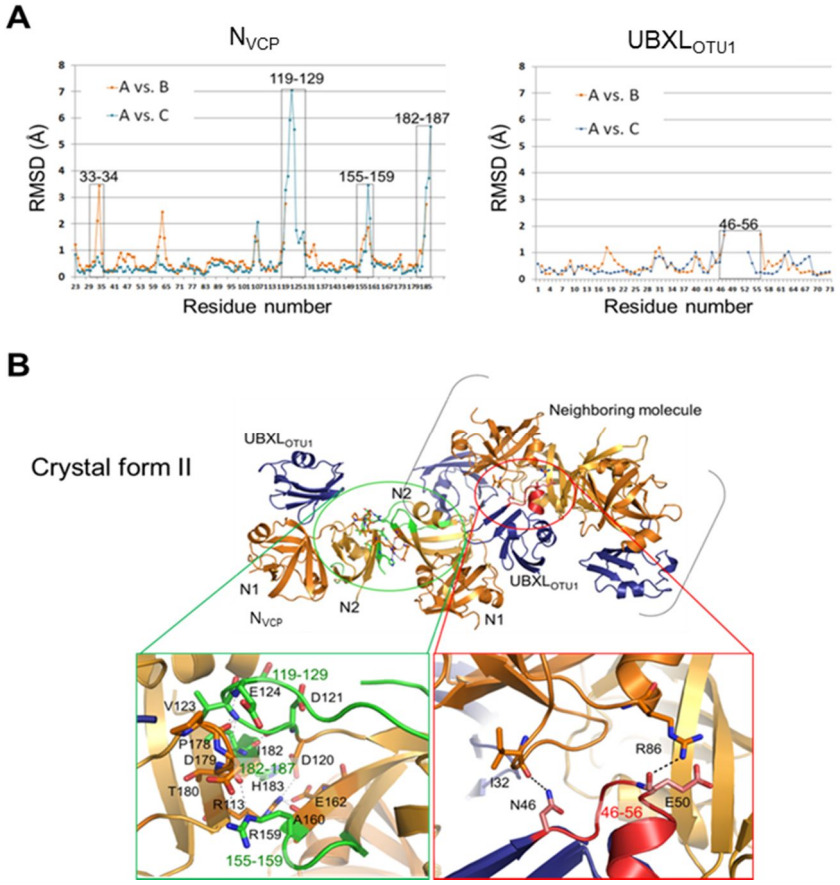

Figure 9. Comparison of Molecules in Two Crystal Forms

(A) Plots of RMSD for the Cα atoms versus residue number for N_{VCP} (left) and $UBXL_{OTU1}$ (right). Regions with large differences are indicated by black boxes. (B) Regions with large differences in A are due to crystal packing in crystal form II. The differences seen in N_{VCP} occur at the interface between N2 domains of two VCP molecules in the asymmetric unit of crystal form II, while the difference seen in $UBXL_{OTU1}$ is due to the interaction with neighboring VCP molecule. They are highlighted in green and red boxes. Hydrogen bonds between the neighboring molecules are marked by dashed line.

3.3. Comparison of $UBXL_{OTU1}$ with UBX_{FAF1}/ UBD_{NPL4}

A DALI search using $UBXL_{OTU1}$ as a search model gave the UBX_{FAF1} (Protein Data Bank code 3QX1) as the closest match with a *Z*-score of 8.8, an RMSD value of 1.9 Å (68 Cα atoms), and sequence identity of 13%. FAF1 is a ubiquitin receptor containing multiple ubiquitin-related domains that is involved in various physiological functions such as apoptosis and NF-κB signaling. The second best match was ubiquitin (Bang et al., 2005; Protein Data Bank code 1YIW) with a *Z*-score of 8.2, an RMSD value of 2.2 Å (63 Cα atoms), and sequence identity of 12%. Other ubiquitin-like proteins such as NEDD8 (Protein Data Bank code 3GZN), SUMO-1 (Protein Data Bank code 1A5R), SMT3 (Protein Data Bank code 3V62), and FUB1 (Protein Data Bank code 2L7R) showed *Z*-scores slightly less than 8, and they all had similar sequence identities as well. UBD of NPL4-like protein (Protein Data Bank code 1WF9) showed a *Z*-score of around 5. Although the function of NPL4-like protein is not yet clear, UBD of NPL4 (Isaacson et al., 2007; Protein Data Bank code 2PJH; UBD_{NPL4}) has been reported to assist VCP along with UFD1 in ERAD (Bebeacua et al., 2012). Thus, it is included in the following comparison instead.

Figures 10 and 11 show a comparison of $UBXL_{OTU1}$ with UBX_{FAF1} (Hänzelmann et al., 2011; Protein Data Bank code 3QQ8) and UBD_{NPL4} along with the structure-based sequence alignment using the alignment program STRAP (Gille et al., 2003). The RMSD value obtained in the superposition of $UBXL_{OTU1}$ and UBX_{FAF1} (UBD_{NPL4}) is 2.21 Å (3.97 Å) for 73 Cα atoms. Although these proteins, namely $UBXL_{OTU1}$, UBX_{FAF1}, and UBD_{NPL4}, share structural homology at the Cα level, the electrostatic surfaces are quite different (Figure. 10). The electrostatic surface of $UBXL_{OTU1}$ is particularly distinct: one side shows a positively charged patch, whereas the opposite side shows a broad negatively charged patch. The positively charged patch is formed by Lys2, Lys4, Arg37, Arg44, and Lys69 from the various strands of the β-sheet, whereas the negatively charged patch is formed by residues such as Asp24, Glu27,

Asp60, and Glu61 from α1 and η1 of $UBXL_{OTU1}$.

Despite the fact that the overall structures are similar, a detailed comparison reveals differences in four regions, and these are highlighted in Figure 11. The four regions are well defined in the electron density maps and are almost the same in all three structures of crystal forms I and II. First, the β1-β2 loop, highlighted the region 1 of Fig. 2A, is tilted more toward the body of the molecule by about 20° in $UBXL_{OTU1}$. Second, the α1 helix of $UBXL_{OTU1}$ is shorter than that of UBX_{FAF1} and UBD_{NPL4} by nearly one turn. This is due to deletion of four residues in $UBXL_{OTU1}$. In addition, $UBXL_{OTU1}$ has an additional α-helix formed by residues 53–56 with an insertion of five residues after β4 (region 4), and this region extends outward from the body of the molecule. In fact, it is about 11 Å away from the corresponding loop position of UBX_{FAF1}. The most intriguing difference is the β3-β4 loop conformation of $UBXL_{OTU1}$ (region 3 in Figure 11). This loop corresponds to the S3/S4 loop, which is part of the signature motif of UBX. This loop is composed of Gly39-Tyr40-Pro41-Pro42, and all the residues are well defined in the electron density map as shown in Figure 11. The two prolines in this loop are found in the *cis*- and *trans*-configurations, respectively (Table 2). The loop has a type VIb β-turn and is stabilized by intramolecular hydrogen bonds formed between Phe38 and Gln43 (N–O, 3.07 Å; O–N, 2.83 Å) as well as π-π stacking interactions between proline and the preceding tyrosine. This is quite similar to that of UBX_{FAF1}; *i.e.* the corresponding Thr-Phe-Pro-Arg forms a VIb β-turn, and the proline adopts a *cis*-configuration. However, the proline of UBX_{FAF1} does not form similar π-π stacking interactions with the preceding phenylalanine, and the distances between the first and the fourth Cα atoms in the loop are 4.96 and 3.80 Å in $UBXL_{OTU1}$ and UBX_{FAF1}, respectively, resulting in different conformations (Figure 11). This may be due to the additional proline in $UBXL_{OTU1}$. Conversely, the proline in the S3/S4 loop of UBX_{p47} was reported to be in trans-configuration (Dreveny et al., 2004). The corresponding region in UBD_{NPL4} is longer by six residues and forms a 3_{10}-helix instead of the loop as shown

in Figure 11. Taken together, the structure of $UBXL_{OTU1}$ exhibits distinctive features from UBX_{FAF1} or UBD_{NPL4}, and these regions, especially regions 1 and 3, appear to serve as a platform for different interactions.

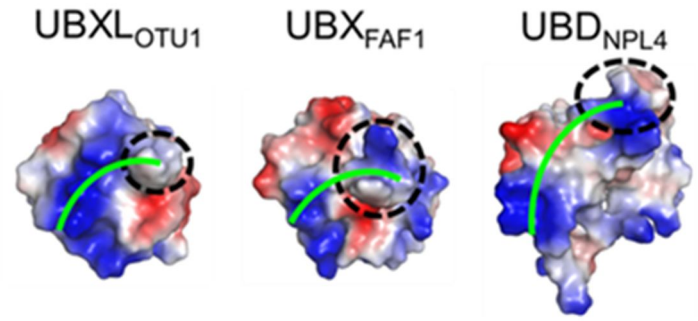

Figure 10. Comparison of the electrostatic potential at UBXL$_{OTU1}$, UBX$_{FAF1}$, and UBD$_{NPL4}$

The surface showing electrostatic charges of UBXL$_{OTU1}$ (left), UBX$_{FAF1}$ (middie), and UBD$_{NPL4}$ (right) at the VCP binding interface with red representing negatively charged surface and blue representing positively charged surface. The S3/S4 loop of UBXL$_{OTU1}$, UBX$_{FAF1}$, and 3_{10}-helix of UBD$_{NPL4}$ are indicated by black dashed circle, and the binding region for N_{VCP} is marked by a green line.

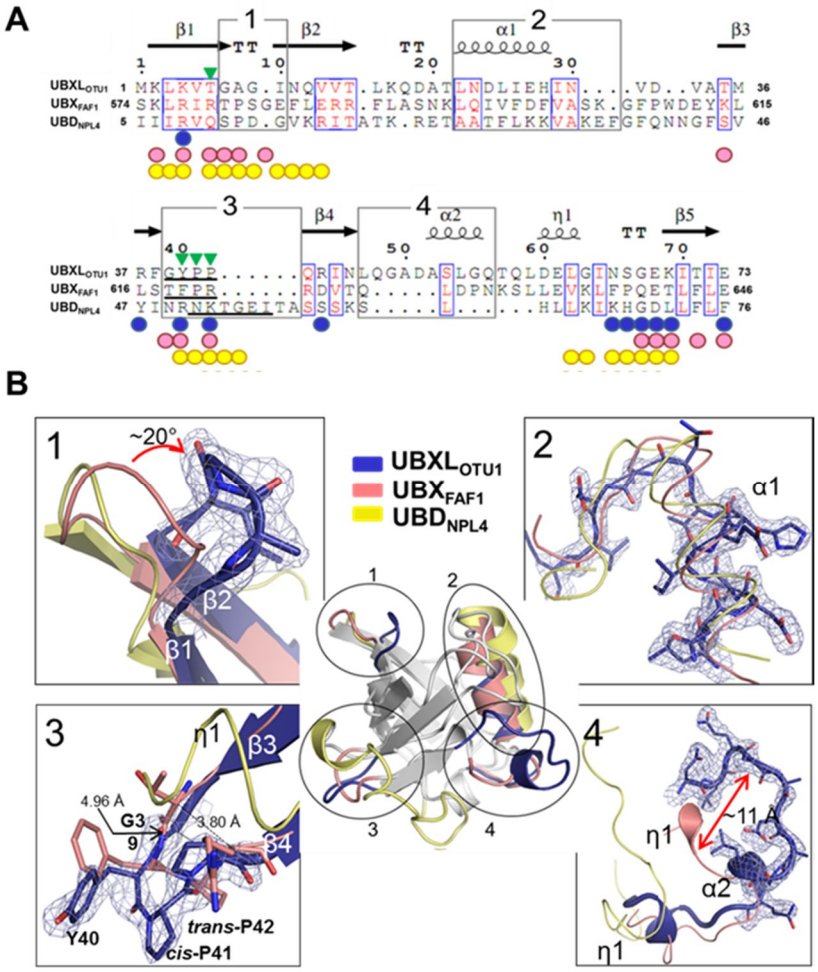

Figure 11. Structural comparison of UBXL$_{OTU1}$, UBX$_{FAF1}$, and UBD$_{NPL4}$

(A) Structure-based sequence alignment of UBXL$_{OTU1}$, UBX$_{FAF1}$, and UBD$_{NPL4}$ with the secondary structural elements of UBXL$_{OTU1}$ shown above the sequence, and α, β, η, and TT denote α-helix, β-strand, 3_{10}-helix, and β-turn, respectively. Well conserved residues are boxed, and the predominant residues shown in red. Residues of the signature motif of UBX are marked by green inverted triangles. The four regions in A are highlighted by boxes. Residues

$UBXL_{OTU1}$ (blue), UBX_{FAF1} (pink), and UBD_{NPL4} (yellow) involved in N_{VCP} binding are indicated by a colored circle below the sequence. The alignment was generated by STRAP (Gille et al., 2003) and ESPript (Gouet et al., 1999). (B) Superposition of $UBXL_{OTU1}$, UBX_{FAF1}, and UBD_{NPL4}. Four regions with significant difference are highlighted in the inserts with the electron density maps ($2F_o - F_c$) of the crystal form I shown at 1.5 σ level. These are highlighted by gray boxes in A.

Table 2. Torsion angles and thermodynamic quantities of local minima for Ac-RFGYPPQR-NHMe

	backbone[a]													
		Ac	Tyr^{40}			Pro^{41}				Pro^{42}				thermodynamic quantity[b]
	conf.[c]	ω_0	ϕ_1	ψ_1	ω_1	ϕ_2	ψ_2	ω_2	χ_2^1	ϕ_3	ψ_3	ω_3	χ_3^1	ΔE
$UBXL_{OTU1}$ from the structure of crystal form I	EcFutFu	160.8	-130.4	134.4	-12.6	-48.6	153.2	178.0	-26.8	-62.0	147.3	-177.1	-20.7	12.49

[a]Units in degrees. [b]Units in kcal/mol. [c]Trans and cis prolyl peptide bonds are represented by "t" and "c", respectively. Down and up puckerings are denoted by subscripts "d" and "u", respectively. The tFd, tFu, cFd, and cFu are represented by td, tu, cd, and cu, respectively.

3.4. Comparison of Interaction between N_{VCP} and $UBXL_{OTU1}$/ UBX_{FAF1}/UBD_{NPL4}

To understand how $UBXL_{OTU1}$ differs from UBX_{FAF1} and UBD_{NPL4} in N_{VCP} binding, the complex structure of N_{VCP} and $UBXL_{OTU1}$ (hereafter referred to as VCP·OTU1) was compared with those of N_{VCP} and UBX_{FAF1} (Hänzelmann et al., 2011; Protein Data Bank code 3QQ8; VCP·FAF1) and N_{VCP} and UBD_{NPL4} (Isaacson et al., 2007; Protein Data Bank code 2PJH; VCP·NPL4). The three complex structures are superposed using only the structures of N_{VCP}. Surprisingly, the three VCP-binding partners are at significantly different positions with respect to each other; *i.e.* they do not overlap at all (Figure. 12). The most pronounced difference is in the position of the α1 helix. The relative positioning of the α1 helix from VCP-binding partners is somewhat different as mentioned above but is significantly different when the complexes are superimposed; *e.g.* in the complex structures, the α1 helix of UBD_{NPL4} is more than 5 Å shifted from that of UBX_{FAF1}, whereas that of $UBXL_{OTU1}$ is somewhat twisted from the other two (Figure 12). The change in accessible surface area (*Δ*ASA) upon complex formation is 590 $Å^2$ for VCP·OTU1; this is much smaller than the corresponding values for VCP·FAF1 and VCP·NPL4, namely 810 and 1,050 $Å^2$, respectively. Also the number of residues involved in the interaction in VCP-OTU1 is much smaller than those found in VCP-FAF1 and VCP-NPL4 (Figure 13). The residues involved in the interaction with N_{VCP} are positioned in three regions, namely β1-β2, β3-β4, and β5, as indicated in Figure 11A.

The molecular surface of N_{VCP} is mapped by interaction of different binding partners (Figure 14). The binding region common to all three VCP-binding partners is colored in brown, the unique surface to $UBXL_{OTU1}$ binding is colored in blue, and the region irrelevant to $UBXL_{OTU1}$, *i.e.* relevant to only UBX and UBD, is colored in green. As seen in Figure 13, interaction in the three complexes is in the same general region, but there are clear differences. In particular, Ser37 and Arg144 of N_{VCP} are only specific to $UBXL_{OTU1}$ binding. They make

non-bonded contacts with Tyr40 of $UBXL_{OTU1}$, which makes a hydrogen bond to the side chain of Asp35 of N_{VCP} (Figure 15). Interestingly, Tyr40 is part of the S3/S4 loop. On the other hand, the green region involves residues from the β6-β7 and β11-β12 loops of N_{VCP} that comprise mainly hydrophobic residues. They interact with the residues from the β1-β2 loop of UBX_{FAF1} and UBD_{NPL4}, *i.e.* region 1 (Figure 11). However, the β1-β2 loop of $UBXL_{OTU1}$ clearly adopts a different conformation from the other two (Figure 11B) and does not make any interactions with N_{VCP}, whereas there are numerous interactions involving both hydrophobic and polar residues between N_{VCP} and UBX_{FAF1} (or UBD_{NPL4}) (Figure 14B).

The primary interaction is via the S3/S4 loop of $UBXL_{OTU1}$ as in UBX (Figure 15). However, binding of $UBXL_{OTU1}$ is somewhat different as the aromatic ring of Tyr40 of $UBXL_{OTU1}$ is packed against the following *cis*-Pro41 on one side and by the side chains of Val38 and Leu72 of N_{VCP} on the other side. Also, Tyr40 is positioned further between the N1 and N2 domains of N_{VCP}, the hydroxyl oxygen of which makes hydrogen bonds with the carboxyl oxygens of Asp35 (2.76 and 3.29 Å) of N_{VCP} (Figure 15). In addition, arginine in the signature motif of UBX is replaced by threonine in $UBXL_{OTU1}$ and does not seem to be conserved. In the case of VCP·FAF1, the corresponding residue Phe619 of UBX_{FAF1} is packed by Val38 and Ile70 of N_{VCP} on one side, and its carbonyl oxygen makes a hydrogen bond with Arg53 of N_{VCP} (3.23 Å). The guanidinium group of Arg621 of UBX_{FAF1} makes hydrogen bonds to the carbonyl oxygens of Pro137 (3.31 Å) and Leu141 (2.52 Å) of N_{VCP}. Alternatively, in UBD_{NPL4}, a 3_{10}-helix is formed instead of the S3/S4 loop found in UBX_{FAF1} and $UBXL_{OTU1}$, and this facilitates N_{VCP} binding (Figure 15). Another major interaction region involves the C-terminal region of the binding partners (Figure 11A). They interact with Phe52, Arg53, Gly54, and Asp55 of N_{VCP}, which is colored in brown (Figure 14A). As seen in the figure, this region is equally important. However, the degree of interactions varies per the three complex structures. For example, Arg53 of N_{VCP} makes six hydrogen bonds in VCP·OTU1, whereas the same

residue of N_{VCP} forms only three and two hydrogen bonds in VCP·FAF1 and VCP·NPL4, respectively. Taken together, our data show that $UBXL_{OTU1}$ binds in a similar position of N_{VCP} as UBX_{FAF1} and UBD_{NPL4}, but the interaction mode is specific unlike the others. This implies that OTU1 is a particular binding partner of VCP.

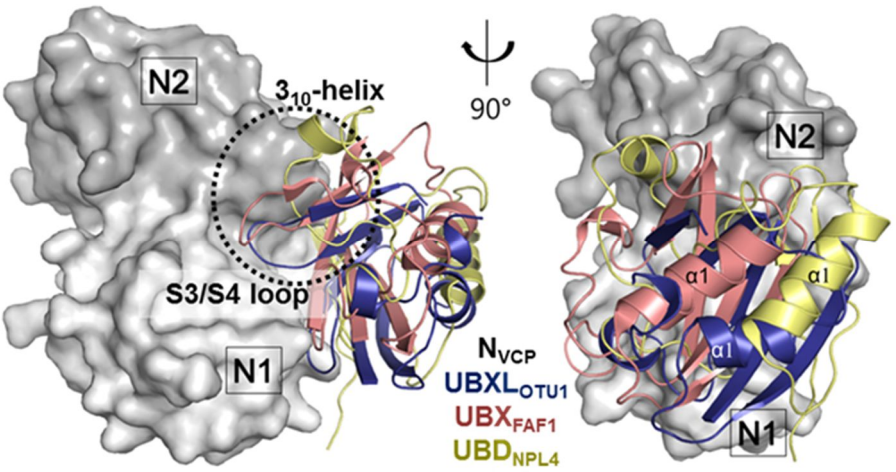

Figure 12. Comparison of interaction between N_{VCP} and binding partners

Superposition of three complex structures: VCP·OTU1 (crystal form I in this study), VCP·FAF1 (Hänzelmann et al., 2011; Protein Data Bank code 3QQ8), and VCP·NPL4 (Isaacson et al., 2007; Protein Data Bank code 2PJH) shown in blue, pink, and yellow, respectively. Only N_{VCP} was used for superposition. N_{VCP} is shown in surface representation, whereas binding partners are shown in ribbon representation. The S3/S4 loop of $UBXL_{OTU1}$ and UBX_{FAF1}, 3_{10}-helix of UBD_{NPL4} are indicated by black dashed circle.

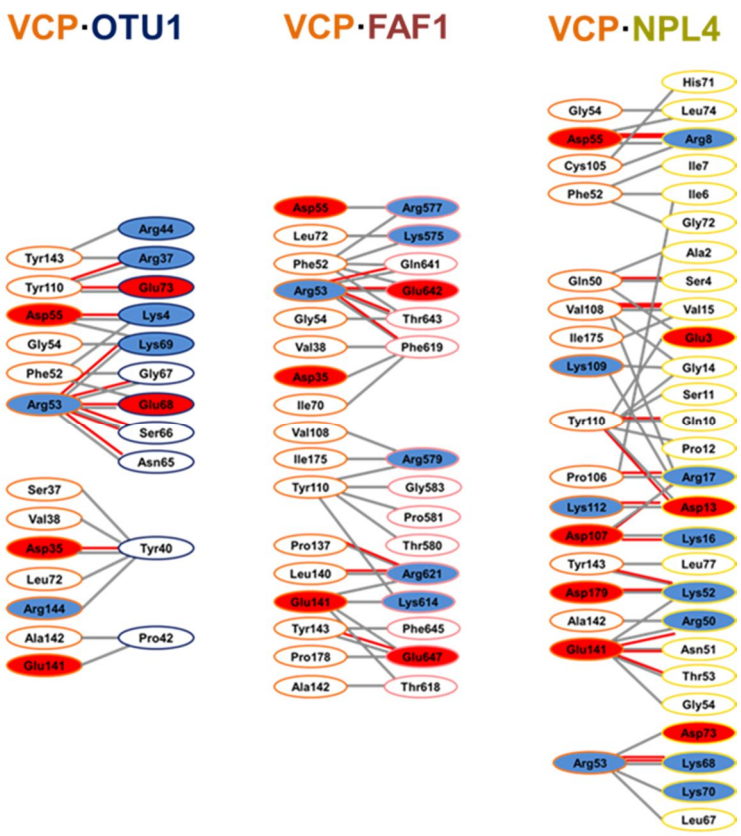

Figure 13. Molecular interaction between VCP and binding partners

Binding residues of VCP and binding partners are shown on the left and right, respectively. Details of the individual residue-residue interactions across interfaces of three complexes analyzed with PDBsum (http://www.ebi.ac.uk/pdbsum/). Negatively charged residues are represented by red circle while blue represent positively charged residues. Gray lines indicate the hydrogen bonds (2.6-3.4 Å) while by red lines represent the hydrophobic interactions (contact within <5.0 Å).

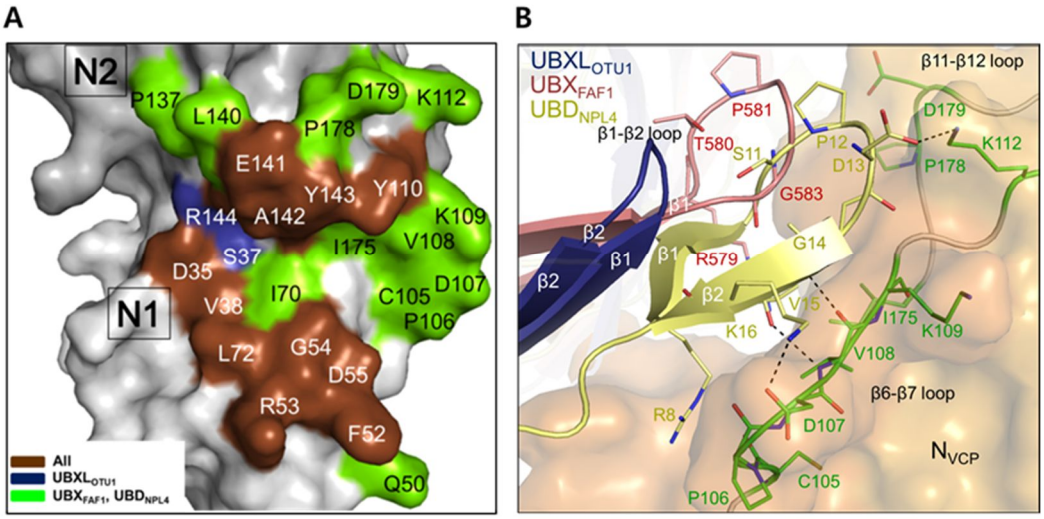

Figure 14. Comparison of binding to VCP within three complexes, VCP·OTU1, VCP·FAF1, and VCP·NPL4

(A) Binding surface of N_{VCP}. Common binding region for all three binding partners is colored in brown, whereas the region unique to $UBXL_{OTU1}$ is colored in blue, and the region that is irrelevant to $UBXL_{OTU1}$ binding but important in UBX_{FAF1} or UBD_{NPL4} binding is shown in green. (B) Interaction between the β1-β2 loop of the binding partners and N_{VCP}. N_{VCP} is depicted in a surface representation. Residues of binding partners involved in the interaction are shown in stick representation with the residues of N_{VCP} in green. Hydrogen bonds are indicated by dashed lines.

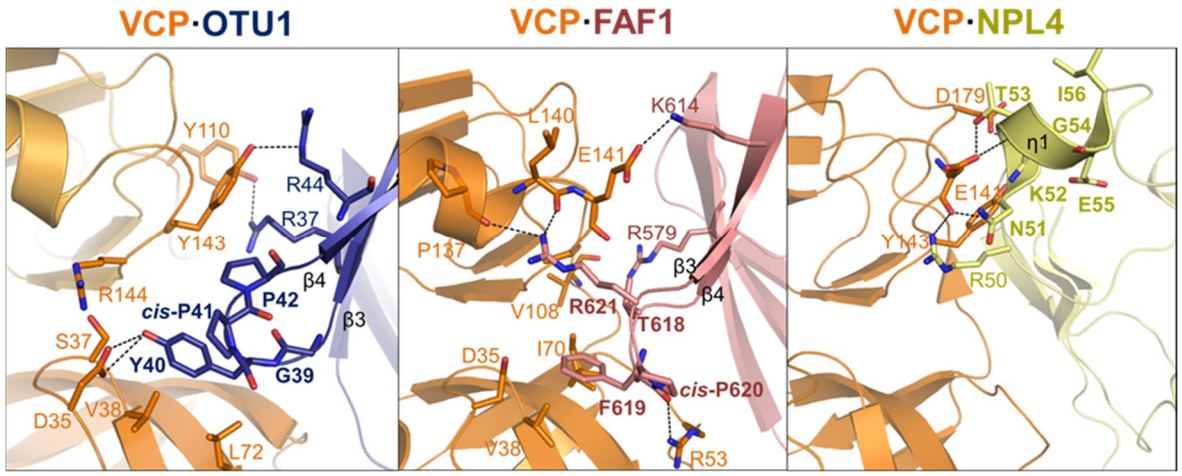

Figure 15. Details of the interaction between VCP and binding partners

The interactions formed around the S3/S4 loop region (in boldface) of binding partners are shown with the key residues in stick presentation. Hydrogen bonds are indicated by dashed lines.

3.5. The S3/S4 Loop of OTU1 Critical for VCP Binding and ERAD

To confirm the importance of the S3/S4 loop of OTU1 in VCP binding based on the complex structure, the mutant was made by using the full-length OTU1. The S3/S4 loop of OTU1 was replaced with that of FAF1, which which showed the closest resemblance as shown above; *i.e.* the mutant (OTU1 ^{39}TFPR^{42}) has the S3/S4 loop sequence corresponding to Thr^{618}-Phe-Pro-Arg^{621} of FAF1. The interactions between the full-length VCP and OTU1 were measured using ITC, and the results are shown in Figure 16. The binding affinity (K_D) between VCP and OTU1 WT is 0.71 μM, whereas the corresponding value for OTU1 ^{39}TFPR^{42} could not be measured possibly due to weak binding. This could be understood based on the modeling study, which showed physical clashes with N_{VCP} when the Gly-Tyr-Pro-Pro loop of OTU1 was replaced by Thr-Phe-Pro-Arg (data now shown). In addition, the two prolines in the S3/S4 loop of OTU1 may impose rigidity in the backbone conformation and prevent conformational changes from propagating to the rest of the protein. The substitution of proline with other residues such as glycine or arginine relieves the rigidity of the backbone and increases the flexibility of the loop. Therefore, forming a negative loop of $UBXL_{OTU1}$ leads to low binding affinity between VCP and OTU1. The substrate degradation assay was carried out to check whether the inability of OTU1 binding to VCP has any influence on the ERAD pathway using ribophorin I (RPN-I^{N299T}) as an ERAD substrate. Degradation of the substrate was monitored in the presence of cycloheximide (de Virgilio et al., 1999). OTU1 ^{39}TFPR^{42} showed relatively reduced degradation and accumulation of RPN-I^{N299T} in comparison with OTU1 WT (Figure 17). This result shows that disruption of the association between VCP and OTU1 leads to the negative regulation of the ERAD pathway; thus, the S3/S4 loop of OTU1 is highly specific and is involved in a unique association with VCP.

It has been reported previously that abrogation of the deubiquitinating activity of OTU1 resulted in impairment of the degradation of misfolded RI332 as an ERAD substrate,

suggesting that OTU1 positively regulates ERAD (Emst et al., 2009). Here, although $UBXL_{OTU1}$ has no relation to the enzymatic activity of OTU1, disruption of the interaction between VCP and OTU1 led to defects in the degradation of ERAD substrates. Therefore, it seems that $UBXL_{OTU1}$ is required for ERAD. Likewise, recent reports have suggested the importance of the association of VCP and UBX proteins. For instance, the S3/S4 loop mutant of UBX_{FAF1} lost the ability to interact with VCP as well as with ubiquitinated substrate via its ubiquitin-associated domain, resulting in the accumulation of substrate (Lee et al., 2013). Another example is UBXD7, which separately binds both VCP and substrate HIF1α and recruits the substrate to VCP for degradation. However, its UBX-lacking mutant could not interact with both VCP and substrate, thus leading to a defect in the degradation of HIF1α (Alexandru et al., 2008). Therefore, the association of UBX proteins with VCP is involved in their function; *i.e.* binding of OTU1 to VCP is needed to activate OTU1 in the ERAD pathway, demonstrating the importance of $UBXL_{OTU1}$. Furthermore, the S3/S4 loop of OTU1 is conserved as residues Gly-Tyr/Phe-Pro-Pro are found in other OTU1 homologs and VCP complex-interacting protein of 135 kDa (VCIP135) which is another known UBXL-containing protein (Figure 18; Uchiyama et al., 2002; Uchiyama et al., 2006). Therefore, not only VCIP135 but also OTU1 homologs are expected to bind VCP in the same manner shown in this study.

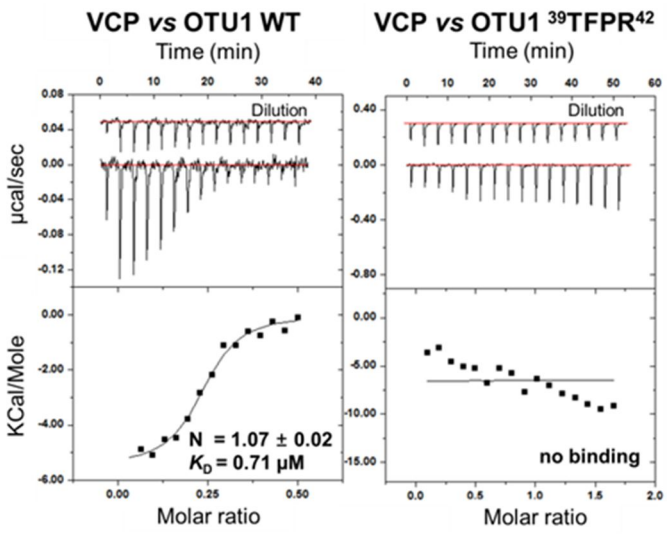

Figure 16. Binding assay for OTU1 wild type and ^{39}TFPR^{42} mutant

ITC raw data and fitted data are for the interaction between the full-length VCP and OTU1. The raw data are shown for injection of OTU1 WT (left), ^{39}TFPR^{42} (right), and a dilution control of OTU1 in buffer (curves on the top are offset for clarity). The lower panels show the integrated heat data against the molar ratio of VCP to OTU1. The closed squares were fitted to a one-site model, and the solid lines represent the best fit results. No measurable interaction was detected between VCP and OTU1 ^{39}TFPR^{42}.

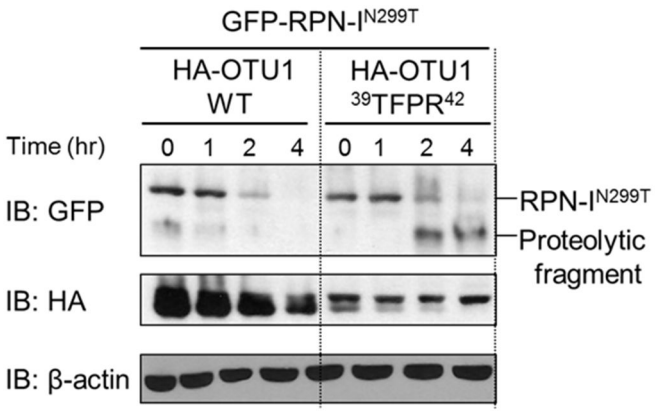

Figure 17. Substrate degradation assay for OTU1 wild type and ^{39}TFPR^{42} mutant

Influences of OTU1 on degradation of RPN-I^{N299T}. Left, OTU1 WT; right; OTU1 ^{39}TFPR^{42}. Substrate was totally degraded in the case of OTU1 WT, whereas the degradation process was retarded, resulting in proteolytic fragments, when the S3/S4 loop was mutated. IB, immunoblot.

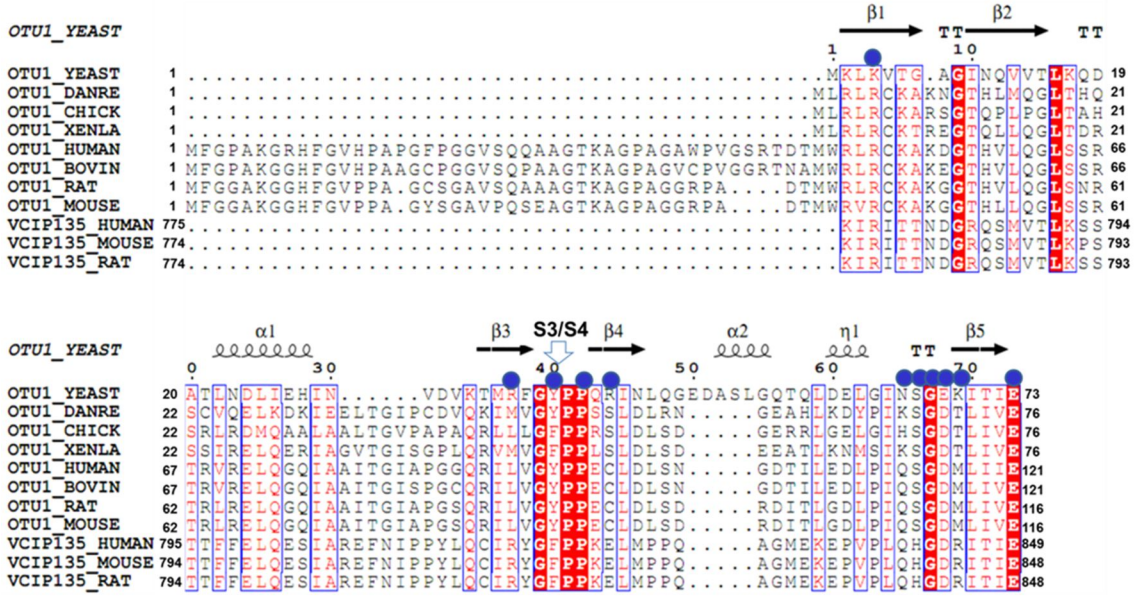

Figure 18. Multiple sequence alignments of $UBXL_{OTU1}$ and other OTU1 homologs and VCIP135 homologs

$UBXL_{OTU1}$ from *Saccharomyces cerevisiae*, *Danio rerio, Gallus gallus, Xenopus laevis, Homo sapiens, Bos taurus, Rattus norvegicus*, and *Mus musculus* with the UBXL domain of VCIP135 from *Homo sapiens, Mus musculus*, and *Rattus norvegicus* using ClustalW (http://embnet.vital-it.ch/software/ClustalW.html). Strictly conserved residues are highlighted with red shaded

boxes, and well-conserved residues are boxed, with the predominant residues shown in red. Secondary structural elements of OTU1 are shown that α, β, and η denote α-helix, β-strand, and 3_{10}-helix, respectively. Residues of $UBXL_{OTU1}$ are involved in VCP binding are indicated by blue circle above the sequence.

3.6. Interaction between the Full-length Proteins

Because VCP exists as a homohexamer, it can possibly bind six different binding partners. Therefore, it is important to characterize the stoichiometry and interaction between the full-length VCP and its binding partners. To determine the stoichiometry of VCP and OTU1, an EM study was carried out. First, gold labeling was carried out using a hexahistidine tag. The tag was added to the C terminus of OTU1 because its N-terminal domain binds to VCP. Negative staining EM images of VCP alone and in complex with the gold-labeled OTU1 were taken. About 5,800 single particles were selected from individual micrographs, and the stoichiometry between VCP and OTU1 was analyzed statistically by counting the number of gold particles. Approximately 80% of the selected particles had one gold particle, and about 15% had two (Figure 19A). The remaining 5% were particles with more than three gold particles (data not shown). Then images of the complex of the full-length proteins (VCP/OTU1 complex) were taken without gold labeling to avoid the restrictive space constraints due to the gold particle, which has a diameter of 5 nm. Three types of negative staining solutions were tried, but methylamine vanadate, pH 8.0 gave the best result as shown in Figure 19B. A total of 2,452 particles of VCP/OTU1 complex were separated successfully from 2,839 particles of a mixture containing VCP alone and VCP/OTU1 complex with the class average. When uranyl formate was used, the ratio between the complex and VCP alone was almost 1,134 to 4,231 possibly due to the acidic nature of the solution, namely pH 5.5 (data not shown). Representative two-dimensional class averages for VCP alone and VCP/OTU1 complex are shown in Figure 19B, which clearly shows that one OTU1 molecule binds to one vertex of homohexameric VCP. ITC measurement using the full-length VCP and OTU1 showed a binding stoichiometry of n = 1.07 ± 0.02 and a K_D of 0.71 μM, suggesting that the stoichiometry of OTU1 to VCP is near 1:6. This is in good agreement with the EM data above. In addition, when $UBXL_{OTU1}$ was removed (data not shown) or mutated (Figure 16), it did not show measurable binding to VCP. This

confirmed again that $UBXL_{OTU1}$ is necessary for binding to VCP.

The stoichiometries between VCP and various binding partners have been reported. In the case of UFD1/NPL4, EM studies clearly show that one UFD1/NPL4 binds one VCP hexamer (Pye et al., 2007; Bebeacua et al., 2012). On the contrary, for both p47 and UBXD1, three molecules of each bind to one VCP hexamer (Beuron et al., 2006; Hänzelmann and Schindelin, 2011). Interestingly, in the case of both FAF1 and UBXD7, one molecule binds one VCP hexamer only when UFD1/NPL4 is prebound to VCP (Hänzelmann et al., 2011; Lee et al., 2013). The K_D values of VCP and its binding partners are 1.7 μM for UFD1/NPL4 (Hänzelmann et al., 2011), 2.3 μM for FAF1 (Hänzelmann et al., 2011), 3.1 μM for UBXD7 (Hänzelmann et al., 2011), and 0.5 μM for p47 (Beuron et al., 2006). These values are comparable with what have seen with OTU1. It is worthwhile mentioning that in some cases bipartite binding has been reported. For example, VCP binding of UFD1/NPL4 utilizes the BS1 segment, which is a short hydrophobic stretch in the C-terminal domain of UFD1, in addition to the UBD of NPL4 as described above (Bruderer et al., 2004). Also, p47 uses a shp1-eyc-p47 domain, which is in the middle of p47, in addition to the C-terminal UBX domain. The shp1-eyc-p47 domain is reported to form a trimer and binds at the interface between the N and D1 domains of VCP. Besides the hierarchical binding of VCP-binding partners, some binding partners such as UFD1/NPL4, p47, and UBXD1 are reported to show mutually exclusive binding (Kern et al., 2009; Chia et al., 2012), whereas others such as UFD1/NPL4 and UBX4 show simultaneous binding (Alberts et al., 2009). This is understandable considering the existence of numerous binding partners and the diverse functions of VCP. Although the crystal structure of truncated proteins showed 1:1 binding between $UBXL_{OTU1}$ and N_{VCP}, the EM study using the full-length proteins clearly showed that one OTU1 binds to the hexameric VCP, suggesting only one OTU1 molecule is sufficient to perform its function; furthermore, it may function with other binding partners.

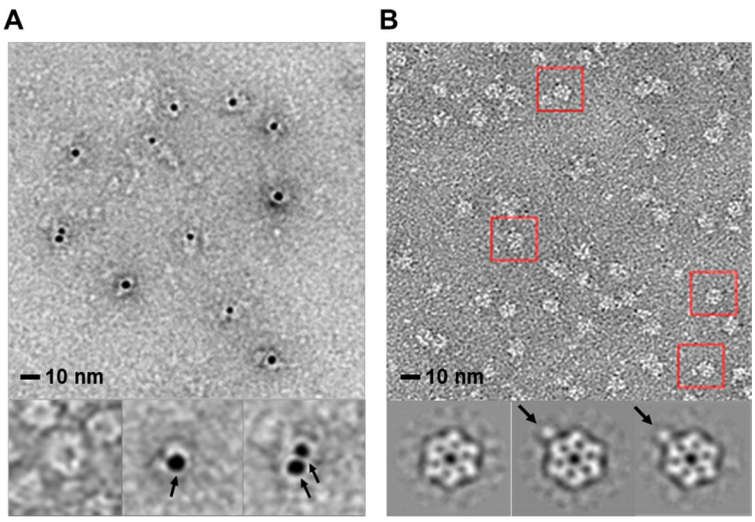

Figure 19. Negative staining electron microscopy analysis on single particle of the VCP and OTU1 complex

(A) Raw images of VCP complexed with gold-labeled OTU1. Bottom panels show VCP with no label as a control (left) and particles with one (middle) and two (right) gold particles with black arrows indicating the gold particle. (B) Electron micrograph of the VCP and OTU1 complex. The bottom panel shows the representative two-dimensional class average for VCP alone (left) and VCP/OTU1 complex (middle and right). VCP/OTU1 complex is marked by a red box. The arrow indicates the OTU1 molecule.

3.7. Dependency of OTU1 Binding to VCP on VCP Adaptor Proteins UFD1/NPL4

UFD1/NPL4 plays a crucial role in ERAD together with VCP, and some VCP-binding partners show hierarchical binding as well as mutually exclusive binding to VCP. The binding pattern for VCP between OTU1 and UFD1/NPL4 was tested using size exclusion chromatography and ITC, and the results are shown in Figure 20. A GST-tagged OTU1 (GST-OTU1) was used to avoid possible confusion caused by molecular weights on size exclusion chromatography and SDS-PAGE. Two sets of experiments were carried out. First, GST-OTU1 was added to VCP alone, and then UFD1/NPL4 was added. Second, UFD1/NPL4 was added to VCP alone, and then OTU1 was added. As expected, both OTU1 and UFD1/NPL4 form a complex with VCP alone, but in addition, both form a quaternary complex, i.e. VCP·GST-OTU1·UFD1/NPL4 (Figure 20). ITC measurements were further determined the binding affinities and the stoichiometries between these, and the results are shown in Figure 21. First, UFD1/NPL4 and premade VCP/OTU1 binary complex showed an apparent K_D of 3.50 μM and n = 1.05 ± 0.17, whereas OTU1 and premade VCP·UFD1/NPL4 ternary complex gave a K_D of 0.41 μM and n = 1.09 ± 0.02. Both suggest that there is 1:1 binding. Interestingly, the K_D values are similar to those obtained for VCP alone; *e.g.* the K_D for UFD1/NPL4 binding to VCP was reported as 1.7 μM (Hänzelmann et al., 2011), and the K_D for OTU1 binding to VCP was 0.71 μM (Figure 16). This clearly shows that VCP can bind OTU1 in both the presence and absence of UFD1/NPL4 and vice versa.

3.8. Accession Number

Coordinates and structure factors have been deposited in the Protein Data Bank under ID codes 4KDL and 4KDI for crystal form I and II, respectively.

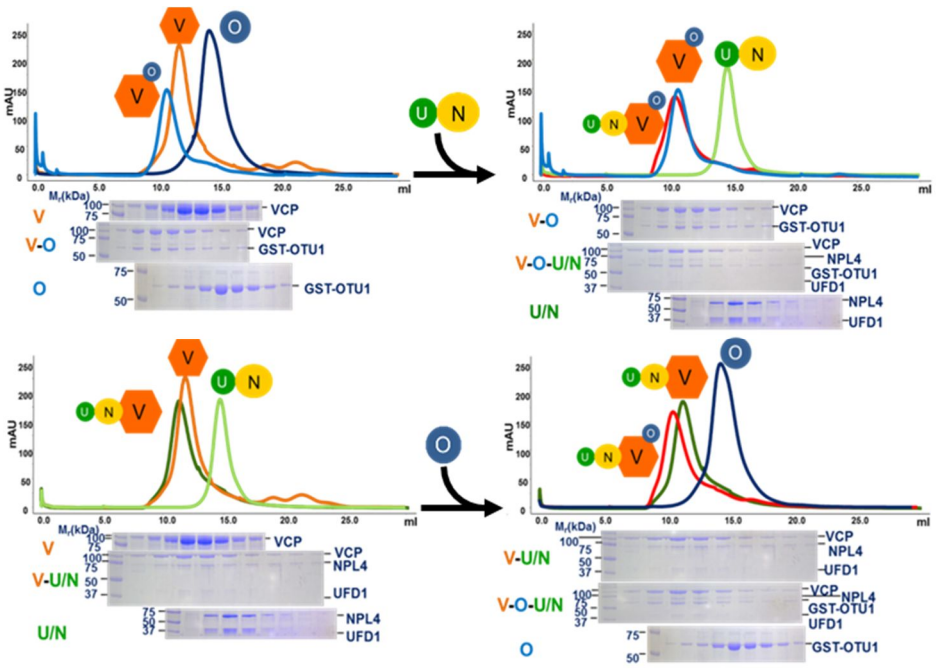

Figure 20. Size exclusion chromatography profile of VCP, OTU1, and UFD1/NPL4

Size exclusion chromatography profile and Coomassie-stained SDS-PAGE of fractions of VCP, GST-OTU1, and UFD1/NPL4. To hexameric VCP, GST-OTU1 and UFD1/NPL4 (top) and UFD1/NPL4 and GST-OTU1 (bottom) were added. SDS-PAGE fractions are shown below the chromatograms. V, O, U, and N stand for VCP, OTU1, UFD1, and NPL4.

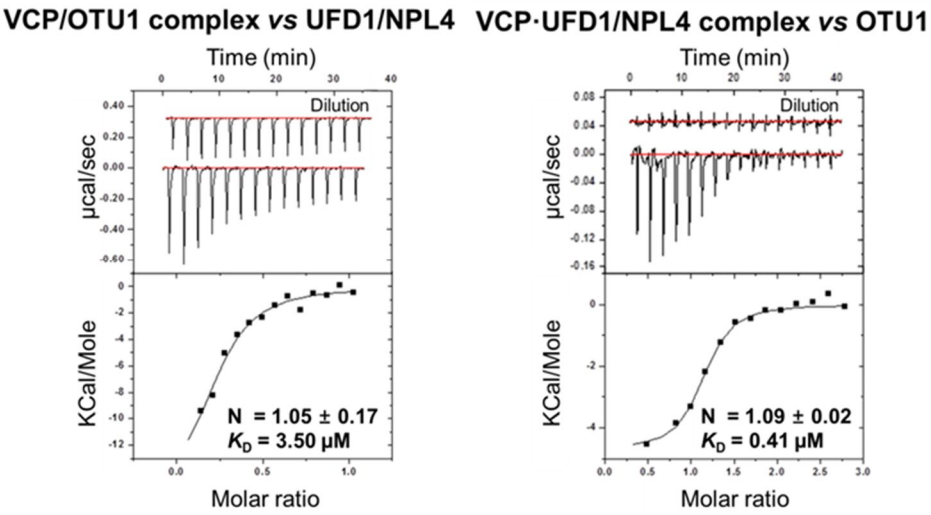

Figure 21. Binding assay of VCP, OTU1, and UFD1/NPL4

ITC binding data for UFD1/NPL4 binding to VCP/OTU1 complex (left) and for OTU1 binding to VCP·UFD1/NPL4 complex (right). mAU, milli-absorbance units.

4. Conclusion

The present study provides the structural basis for the interaction between VCP and OTU1, and shown that this interaction is importantly mediated by the S3/S4 loop of OTU1. One OTU1 molecule binds to one VCP hexamer with similar binding affinity both in the presence and absence of UFD1/NPL4. The $UBXL_{OTU1}$ binds at the interface between the two subdomains (N1 and N2) of VCP. In particular, the conformation of the Gly39-Tyr40-*cis*-Pro41-Pro42 loop of $UBXL^{OTU1}$ is critical for N_{VCP} binding. Although some of these properties of UBXL mimic UBX, the interaction is quite specific and has direct bearing on the proteasomal degradation of ERAD substrates. Based on these results, it is plausible that OTU1 can participate in the regulation of ubiquitinated substrates in both UFD1/NPL4-dependent and -independent manners. Our data provide insights into the interaction between the full-length VCP and OTU1 as well as the interaction between N_{VCP} and $UBXL_{OTU1}$ that could be applicable to other UBXL-containing proteins.

5. References

Alberts S. M., Sonntag C., Schäfer A., Wolf D. H. (2009) Ubx4 modulates cdc48 activity and influences degradation of misfolded proteins of the endoplasmic reticulum. J. Biol. Chem. 284, 16082–16089.

Alexandru,G., Graumann, J., Smith, G.T., Kolawa, N.J., Fang, R., Deshaies, R.J. (2008) UBXD7 binds multiple ubiquitin ligases and implicates p97 in HIF1alpha turnover. Cell, **134**:804-816.

Bagola, K., Mehnert, M., Jarosch, E., and Sommer, T. (2011) Protein dislocation from the ER. Biochim. Biophys. Acta, **1808**:925-936.

Ballar, P., Shen, Y., Yang, H., and Fang, S. (2006) The role of a novel p97/valosin-containing protein-interacting motif of gp78 in endoplasmic reticulum-associated degradation. J. Biol. Chem. **281**:35359-35368.

Bang, D., Makhatadze, G.I., Tereshko, V., Kossiakoff, A.A., and Kent, S.B. (2005) Total chemical synthesis and X-ray crystal structure of a protein diastereomer: [D-Gln35] ubiquitin. Angew. Chem. Int. Ed. Engl. **44**:3852-3856.

Bebeacua, C., Förster, A., McKeown, C., Meyer, H.H., Zhang, X., and Freemont, P.S. (2012) Distinct conformations of the protein complex p97-Ufd1-Npl4 revealed by electron cryomicroscopy. Proc. Natl. Acad. Sci. USA, **109**:1098-1103.

Beuron, F., Dreveny, I., Yuan, X., Pye, V.E., McKeown, C., Briggs, L C., Cliff, M.J., Kaneko, Y., Wallis, R., Isaacson, R.L., Ladbury, J.E, Matthews, S.J., Kondo, H., Zhang, X., and Freemont, P.S. (2006) Conformational changes in the AAA ATPase p97-p47 adaptor complex. EMBO J. **25**:1967-1976.

Boeddrich, A., Gaumer, S., Haacke, A., Tzvetkov, N., Albrecht, M., Evert, B.O., Müller, E.C.,

Lurz, R., Breuer, P., Schugardt, N., Plassmann, S., Xu, K., Warrick, J.M., Suopanki, J., Wüllner, U., Frank, R., Hartl, U.F., Bonini, N.M., and Wanker, E.E. (2006) An arginine/lysine-rich motif is crucial for VCP/p97-mediated modulation of ataxin-3 fibrillogenesis. EMBO J. **25**:1547-1558.

Bruderer, R.M., Brasseur, C., and Meyer, H.H. (2004) The AAA ATPase p97/VCP interacts with its alternative co-factors, Ufd1-Npl4 and p47, through a common bipartite binding mechanism. J. Biol. Chem. **279**:49609-49616.

Brunger, A.T., Adams, P.D., Clore, G.M., DeLano, W.L., Gros, P., Grosse-Kunstleve, R.W., Jiang, J.S., Kuszewski, J., Nilges, M., Pannu, N.S., Read, R.J., Rice, L.M., Simonson, T., and Warren, G.L. (1998) Crystallography & NMR system: A new software suite for macromolecular structure determination. Acta Crystallogr. D Biol. Crystallogr. **54**:905–921.

Buchberger, A. (2010) Control of ubiquitin conjugation by cdc48 and its cofactors. Subcell Biochem. **54**:17-30.

Carvalho, P., Goder, V., and Rapoport, T.A. (2006) Distinct ubiquitin-ligase complexes define convergent pathways for the degradation of ER proteins. Cell, **126**:361-373.

Chapman, E., Fry, A.N., and Kang, M. (2011) The complexities of p97 function in health and disease. Mol. Biosyst. **7**:700-710.

Chia W. S., Chia D. X., Rao F., Bar Nun S., Geifman Shochat S. (2012) ATP binding to p97/VCP D1 domain regulates selective recruitment of adaptors to its proximal N-domain. PLoS One 7, e50490.

DeLaBarre, B., and Brunger, A.T. (2003) Complete structure of p97/valosin-containing protein reveals communication between nucleotide domains. Nat. Struct. Biol. **10**:856-863.

DeLano, W.L. (2002) The PyMOL User's Manual (San Carlos, CA: DeLano Scientific).

de Virgilio, M., Kitzmüller, C., Schwaiger, E., Klein, M., Kreibich, G., and Ivessa, N.E. (1999)

Degradation of a short-lived glycoprotein from the lumen of the endoplasmic reticulum: the role of N-linked glycans and the unfolded protein response. Mol. Biol. Cell, **10**:4059-4073.

de Vrij, F.M., Fischer, D.F., van Leeuwen, F.W., and Hol, E.M. (2004) Protein quality control in Alzheimer's disease by the ubiquitin proteasome system. Prog. Neurobiol. **74**:249-270.

Dreveny, I., Kondo, H., Uchiyama, K., Shaw, A., Zhang, X., and Freemont, P.S. (2004) Structural basis of the interaction between the AAA ATPase p97/VCP and its adaptor protein p47. EMBO J. **23**:1030–1039.

Emsley, P., and Cowtan, K. (2004) Coot: model-building tools for molecular graphics. Acta Crystallogr. D Biol. **60**:2126–2132.

Ernst, R., Mueller, B., Ploegh, H.L., and Schlieker, C. (2009) The otubain YOD1 is a deubiquitinating enzyme that associates with p97 to facilitate protein dislocation from the ER. Mol. Cell, **36**:28–38.

Erzurumlu, Y., Kose, F.A., Gozen, O., Gozuacik, D., Toth, E.A., and Ballar, P. (2013) A unique IBMPFD-related P97/VCP mutation with differential binding pattern and subcellular localization. Int. J. Biochem. Cell Biol. **45**:773-782.

Federovitch, C.M., Ron, D., and Hampton, R.Y. (2005) The dynamic ER: experimental approaches and current questions. Curr. Opin. Cell Biol. **17**:409-414.

Finley, D. (2009) Recognition and processing of ubiquitin-protein conjugates by the proteasome. Annu. Rev. Biochem. **78**:477–513.

Frisch, M.J., Trucks, G.W., Schlegel, H.B., Scuseria, G.E., Robb, M.A., Cheeseman, J.R., Scalmani, G., Barone, V., Mennucci, B., Petersson, G.A., et al. (2009) Gaussian 09, Revision A.02 (Gaussian, Wallingford, CT).

Gille C., Lorenzen S., Michalsky E., Frömmel C. (2003) KISS for STRAP: user extensions for a protein alignment editor. Bioinformatics **19**: 2489–2491.

Goder, V. (2012) Roles of ubiquitin in endoplasmic reticulum-associated protein degradation (ERAD) Curr. Prot. Pep. Sci. **13**:425-435.

Gouet P., Courcelle E., Stuart D.I., Métoz F. (1999) ESPript: analysis of multiple sequence alignments in PostScript. Bioinformatics **15**: 305–308.

Halawani, D., and Latterich. M. (2006) p97: the cell's molecular purgatory? Mol. Cell, **22**:713–717.

Halawani, D., Tessier, S., Anzellotti, D., Bennett, D.A., Latterich, M., and LeBlanc, A.C. (2010) Identification of Caspase-6-mediated processing of the valosin containing protein (p97) in Alzheimer's disease: a novel link to dysfunction in ubiquitin proteasome system-mediated protein degradation. J. Neurosci. **30**:6132-6142.

Hampton, R.Y. (2002) ER-associated degradation in protein quality control and cellular regulation. Curr. Opin. Cell Biol. **14**:476-482.

Hänzelmann, P., Buchberger, A., and Schindelin, H. (2011) Hierarchical binding of cofactors to the AAA ATPase p97. Structure, **19**:833–843.

Hänzelmann P., Schindelin H. (2011) The structural and functional basis of the p97/valosin-containing protein (VCP)-interacting motif (VIM): mutually exclusive binding of cofactors to the N-terminal domain of p97. J. Biol. Chem. 286, 38679–38690.

Hassink, G.C., Zhao, B., Sompallae, R., Altun, M., Gastaldello, S., Zinin, N.V., Masucci, M.G., and Lindsten, K. (2009) The ER-resident ubiquitin-specific protease 19 participates in the UPR and rescues ERAD substrates. EMBO Rep. **10**:755–761.

Hegde, R.S, and Ploegh, H.L. (2010) Quality and quantity control at the endoplasmic reticulum. Curr. Opin. Cell Biol. **22**:437–446.

Hirsch, C., Gauss, R., Horn, S.C., Neuber, O., and Sommer, T. (2009) The ubiquitylation machinery of the endoplasmic reticulum. Nature, **458**:453-460.

Hitt, R., and Wolf, D.H. (2004) Der1p, a protein required for degradation of malfolded soluble

proteins of the endoplasmic reticulum: topology and Der1-like proteins. FEMS Yeast Res. **4**:721-729.

Horn, S.C., Hanna, J., Hirsch, C., Volkwein, C., Schütz, A., Heinemann, U., Sommer, T., and Jarosch, E. (2009) Usa1 functions as a scaffold of the HRD-ubiquitin ligase. Mol. Cell, **36**:782-793.

Huyton, T., Pye, V.E., Briggs, L.C., Flynn, T.C., Beuron, F., Kondo, H., Ma, J., Zhang, X., and Freemont, P. S. (2003) The crystal structure of murine p97/VCP at 3.6 Å. J. Struct. Biol. **144**:337-348.

Isaacson, R.L., Pye, V.E., Simpson, P., Meyer, H.H., Zhang, X., Freemont, P.S., and Matthews, S. (2007) Detailed structural insights into the p97-Npl4-Ufd1 interface. J. Biol. Chem. **282**:21361–21369.

Jarosch, E., Taxis, C., Volkwein, C., Bordallo, J., Finley, D., Wolf, D.H. and Sommer, T. (2002) Protein dislocation from the ER requires polyubiquitination and the AAA-ATPase Cdc48. Nat. Cell Biol. **4**:134–139.

Jentsch, S., and Rumpf, S. (2007). Cdc48 (p97): a "molecular gearbox" in the ubiquitin pathway? Trends Biochem. Sci. **32**:6-11.

Kern M., Fernandez-Sáiz V., Schäfer Z., Buchberger A. (2009) UBXD1 binds p97 through two independent binding sites. Biochem. Biophys. Res. Commun. 380, 303–307.

Kim, I., Ahn, J., Liu, C., Tanabe, K., Apodaca, J., Suzuki, T., and Rao, H. (2006) The Png1-Rad23 complex regulates glycoprotein turnover. J. Cell Biol. **172**:211-219.

Kloppsteck, P., Ewens, C.A., Förster, A., Zhang, X., and Freemont, P.S. (2012) Regulation of p97 in the Ubiquitin–Proteasome System by the UBX protein-family. Biochim. Biophys. Acta, **1823**:125-129.

Laskowski, R.A., MacArthur, M.W., Moss, D.S., and Thornton, J.M. (1993) PROCHECK: a program to check the stereochemical quality of protein structures. J. Appl. Cryst. **26**:283-

291.

Lee, J.J., Park, J.K., Jeong, J., Jeon, H., Yoon, J.B., Kim, E.E., and Lee, K.J. (2013) Complex of Fas-associated factor 1 (FAF1) with valosin-containing protein (VCP)-Npl4-Ufd1 and polyubiquitinated proteins promotes endoplasmic reticulum-associated degradation (ERAD). J. Biol. Chem. **288**:6998-7011.

Levine, T., and Rabouille, C. (2005) Endoplasmic reticulum: one continuous network compartmentalized by extrinsic cues. Curr. Opin. Cell Biol. **17**:362-368.

Lilley, B.N., and Ploegh, H.L. (2004) A membrane protein required for dislocation of misfolded proteins from the ER. Nature, **429**:834-840.

Lim, P.J., Danner, R., Liang, J., Doong, H., Harman, C., Srinivasan, D., Rothenberg, C., Wang, H., Ye, Y., Fang, S., and Monteiro, M.J. (2009) Ubiquilin and p97/VCP bind erasin, forming a complex involved in ERAD. J. Cell Biol. **187**:201–217.

Makarova, K.S., Aravind, L., and Koonin, E.V. (2000) A novel superfamily of predicted cysteine proteases from eukaryotes, viruses and Chlamydia pneumoniae. Trends Biochem. Sci. **25**:50–52.

Marenich, A.V., Cramer, C.J., and Truhlar, D.G. (2009) Universal solvation model based on solute electron density and on a continuum model of the solvent defined by the bulk dielectric constant and atomic surface tensions. J. Phys. Chem. B, **113**:6378-6396.

McCoy, A.J., Grosse-Kunstleve, R.W., Adams, P.D., Winn, M.D., Storoni, L.C., and Read, R.J. (2007) Phaser crystallographic software. J. Appl. Crystallogr. **40**:658-674.

Merulla, J., Fasana, E., Soldà, T., and Molinari, M. (2013) Specificity and regulation of the endoplasmic reticulum-associated degradation machinery. Traffic. **14**(7):767-777.

Messick, T.E., Russell, N.S., Iwata, A.J., Sarachan, K.L., Shiekhattar, R., Shanks, J.R., Reyes-Turcu, F.E., Wilkinson, K.D., and Marmorstein, R. (2008) Structural basis for ubiquitin recognition by the Otu1 ovarian tumor domain protein. J. Biol. Chem. **283**:11038-11049.

Meusser, B., Hirsch, C., Jarosch, E., and Sommer, T. (2005) ERAD: the long road to destruction. Nat. Cell Biol. **7**:766-772.

Mevissen, T.E., Hospenthal, M.K., Geurink, P.P., Elliott, P.R., Akutsu, M., Arnaudo, N., Ekkebus, R., Kulathu, Y., Wauer, T., El Oualid, F., Freund, S.M., Ovaa, H., and Komander, D. (2013) OTU Deubiquitinases Reveal Mechanisms of Linkage Specificity and Enable Ubiquitin Chain Restriction Analysis. Cell, **154**:169-184.

Meyer, H., Bug, M., and Bremer, S. (2012) Emerging functions of the VCP/p97 AAA-ATPase in the ubiquitin system. Nat. Cell Biol. **14**:117-123.

Murshudov, G.N., Vagin, A.A., and Dodson, E.J. (1997) Refinement of macromolecular structure by the maximum-likelihood method. Acta Crystallogr. D Biol. **53**:240–255.

Nakatsukasa, K., Huyer, G., Michaelis, S., and Brodsky, J.L. (2008) Dissecting the ER-associated degradation of a misfolded polytopic membrane protein. Cell, **132**:101-112.

Otwinowski, Z., and Minor, W. (1997) Processing of X-ray diffraction data collected in oscillation mode. Methods Enzymol. **276**:307–326.

Park, S., Isaacson, R., Kim, H.T., Silver, P.A., and Wagner, G. (2005) Ufd1 exhibits the AAA-ATPase fold with two distinct ubiquitin interaction sites. Structure, **13**:995-1005.

Pye V. E., Beuron F., Keetch C. A., McKeown C., Robinson C. V., Meyer H. H., Zhang X., Freemont P. S. (2007) Structural insights into the p97-Ufd1-Npl4 complex. Proc. Natl. Acad. Sci. U.S.A. 104, 467–472.

Raasi, S., and Wolf, D.H. (2007) Ubiquitin receptors and ERAD: a network of pathways to the proteasome. Semin. Cell Dev. Biol. **18**:780-791.

Rape, M., Hoppe, T., Gorr, I., Kalocay, M., Richly, H., and Jentsch, S. (2001) Mobilization of processed, membrane-tethered SPT23 transcription factor by CDC48(UFD1/NPL4), a ubiquitin-selective chaperone. Cell, **107**:667-677.

Rumpf, S., and Jentsch, S. (2006) Functional division of substrate processing cofactors of the

ubiquitin-selective Cdc48 chaperone. Mol. Cell, **21**:261-269.

Sato, B.K., and Hampton, R.Y. (2006) Yeast Derlin Dfm1 interacts with Cdc48 and functions in ER homeostasis. Yeast, **23**:1053-1064.

Sato, B.K., Schulz, D., Do, P.H., and Hampton, R.Y. (2009) Misfolded membrane proteins are specifically recognized by the transmembrane domain of the Hrd1p ubiquitin ligase. Mol. Cell, **34**:212-222.

Schuberth, C., and Buchberger, A. (2008) UBX domain proteins: major regulators of the AAA ATPase Cdc48/p97. Cell. Mol. Life Sci. **65**:2360–2371.

Song, C., Wang, Q., and Li, C.C. (2003) ATPase activity of p97-valosin-containing protein (VCP). D2 mediates the major enzyme activity, and D1 contributes to the heat-induced activity. J. Biol. Chem. **278**:3648-3655.

Tang, G., Peng, L., Baldwin, P.R., Mann, D.S., Jiang, W., Rees, I., and Ludtke, S.J. (2007) EMAN2: an extensible image processing suite for electron microscopy. J. Struct. Biol. **157**:38-46.

Tang, W.K., Li, D., Li, C.C,, and Esser, L., Dai, R., Guo, L., and Xia, D. (2010) A novel ATP-dependent conformation in p97 N-D1 fragment revealed by crystal structures of disease-related mutants. EMBO J. **29**:2217-2229.

Uchiyama, K., Jokitalo, E., Kano, F., Murata, M., Zhang, X., Canas, B., Newman, R., Rabouille, C., Pappin, D., Freemont, P., and Kondo, H. (2002) VCIP135, a novel essential factor for p97/p47-mediated membrane fusion, is required for Golgi and ER assembly in vivo. J. Cell Biol. **159**:855-866.

Uchiyama, K., Totsukawa, G., Puhka, M., Kaneko, Y., Jokitalo, E., Dreveny, I., Beuron, F., Zhang, X., Freemont, P., and Kondo, H. (2006) p37 is a p97 adaptor required for Golgi and ER biogenesis in interphase and at the end of mitosis. Dev. Cell, **11**:803-816.

van Heel, M., Harauz, G., Orlova, E.V., Schmidt, R., and Schatz, M. (1996) A new generation

of the IMAGIC image processing system. J. Struct. Biol. **116**:17-24.

Vashist, S., and Ng, D.T. (2004) Misfolded proteins are sorted by a sequential checkpoint mechanism of ER quality control. J. Cell Biol. **165**:41-52.

Wang, Q., Li, L., and Ye, Y. (2006) Regulation of retrotranslocation by p97-associated deubiquitinating enzyme ataxin-3. J. Cell Biol. **174**:963–971.

Wang, Q., Song, C., and Li, C.C. (2004) Molecular perspectives on p97-VCP: progress in understanding its structure and diverse biological functions. J. Struct. Biol. **146**:44-57.

Wolf, D.H., and Stolz, A. (2012) The Cdc48 machine in endoplasmic reticulum associated protein degradation. Biochim. Biophys. Acta, **1**:117-124.

Woodman, P.G. (2003) p97, a protein coping with multiple identities. J. Cell Sci. **116**:4283-4290.

Xu, P., Duong, D.M., Seyfried, N.T., Cheng, D., Xie, Y., Robert, J., Rush, J., Hochstrasser, M., Finley, D., and Peng, J. (2009) Quantitative proteomics reveals the function of unconventional ubiquitin chains in proteasomal degradation. Cell, **137**:133-145.

Yamanaka, K., Sasagawa, Y., and Ogura, T. (2012) Recent advances in p97/VCP/Cdc48 cellular functions. Biochim. Biophys. Acta, **1823**:130-137.

Ye, Y., Meyer, H.H., and Rapoport, T.A. (2001). The AAA ATPase Cdc48/p97 and its partners transport proteins from the ER into the cytosol. Nature, **414**:652-656.

Ye, Y., Meyer, H.H., and Rapoport, T.A. (2003) Function of the p97-Ufd1-Npl4 complex in retrotranslocation from the ER to the cytosol: dual recognition of nonubiquitinated polypeptide segments and polyubiquitin chains. J. Cell Biol. **162**:71-84.

Yeung, H.O, Kloppsteck, P., Niwa, H., Isaacson, R.L., Matthews, S., Zhang, X., and Freemont, P.S. (2008) Insights into adaptor binding to the AAA protein p97. Biochem. Soc. Trans. **36**:62-67.

Zhang, X., Shaw, A., Bates, P.A., Newman, R.H., Gowen, B., Orlova, E., Gorman, M.A.,

Kondo, H., Dokurno, P., Lally, J., Leonard, G., Meyer, H., van Heel, M., and Freemont, P.S. (2000) Structure of the AAA ATPase p97. Mol. Cell, **6**:1473-1484.

Zhong, X., and Pittman, R.N. (2006) Ataxin-3 binds VCP/p97 and regulates retrotranslocationof ERAD substrates. Hum. Mol. Genet. **15**:2409–2420.

Zwart, P.H., Afonine, P.V., Grosse-Kunstleve, R.W., Hung, L.W., Ioerger, T.R., McCoy, A.J., McKee, E., Moriarty, N.W., Read, R.J., Sacchettini, J.C., Sauter, N.K., Storoni, L.C., Terwilliger, T.C., and Adams, P.D. (2008) Automated structure solution with the PHENIX suite. Methods Mol. Biol. **426**:419-435.

Abstract in Korean

국문초록

Structural Insights into the Interaction between AAA$^+$ ATPase p97/VCP and its Substrate Processing Factor, OTU1

p97/VCP 와 OTU1의 복합체 결정 구조에 관한 연구

생체 내 잘못된 3차 구조를 가진 단백질들이 축적되면 알츠하이머, 파킨슨, 헌팅턴 질환과 같은 다양한 퇴행성 뇌질환 뿐만 아니라 암이 유발될 수 있다. 특히, p97/VCP 유전자 돌연변이가 생기면 inclusion body myopathy, Paget's disease and frontotemporal dementia (IBMPFD)와 더불어 amyotrophic lateral sclerosis (ALS)을 일으킬 수 있다고 보고된 바 있다. 이를 막기 위해 비정상적인 단백질들은 단백질 분해 경로를 통해서 quality control을 유지하게 됩니다. 이 중 유비퀴틴-프로테아좀 시스템을 통해 단백질 분해가 이루어지는 ER-associated degradation (ERAD) 경로가 있다. 이는 ER내의 잘못된 단백질을 인지하고 이를 ER에서 세포질로의 retrotranslocation 과정을 거쳐 마지막으로 프로테아좀에 전달하여 분해시키는 일련의 과정을 말합니다. 이 경로에는 p97/VCP가 필수적이고 다양한 cofactor들이 요구된다. 그 중 OTU1은 ERAD에서 작용하는 탈유비퀴틴화 효소로써 UBX-like (UBXL) 도메인을 통해 p97/VCP와 결합할 수 있다는 보고가 있다. 이 도메인은 기존에 잘 알려진 UBX 도메인과 낮은 서열 동일성을 가졌고, p97/VCP와의 중요 결합 부위로 보존된 signature motif가 없다. 이를 토대로 OTU1의 UBXL 도메인은

UBX 도메인과 다르게 VCP에 결합할 것이라 여겨지지만, 아직 알려진 바 없다. 본 연구에서는 p97/VCP와 그것의 결합 단백질로 알려진 탈유비퀴틴화 효소인 OTU1와의 복합체 삼차원 구조를 규명하였고, mutatagenesis를 통해 ERAD 내에서의 기능을 연구하였다. 더불어 single partice analysis와 ITC assay를 통해 전체적인 구조의 organization을 확인함으로써 p97/VCP의 기능을 좀 더 분명하게 밝힐 수 있었다. 본 연구를 통해 OTU1 한 분자가 p97/VCP hexamer 한 분자에 0.71 μM의 결합력으로 결합함을 확인하였다. 그리고 p97/VCP와 OTU1의 결합체 구조를 통해 OTU1의 UBXL 도메인은 UBX 도메인과 유사한 ubiquitin-like fold를 가지지만, 다른 정전하가 형성된 표면을 가지며 loop의 형태도 다르게 형성됨을 확인할 수 있었다. 이로써 UBX와 다르게 p97/VCP와 결합 양상을 보였다. 특히, p97/VCP와 결합하는 주요 부분인 S3/S4 loop이 OTU1에서만 특이적으로 보존되었음을 발견하였고, p97/VCP와의 결합을 막게되면, ERAD 기질의 분해를 저해한다. 이러한 결과들을 통해 p97/VCP와 UBXL의 새로운 결합 모드를 확인하였고, ERAD 내에서 두 단백질의 제 역할을 하기 위해서는 p97/VCP와 OTU1의 결합이 중요하다는 점을 보여준다.

주요어: ER-associated degradation/ VCP/ OTU1/ Protein-protein interaction/ Crystal structure/ Electron microscopy/ Isothermal titration calorimetry/ Site directed mutagenesis